PHASE SYNCHRONIZATION BETWEEN POLAR CLIMATES: ITS IDENTIFICATION, EVOLUTION, AND CONNECTION TO THE ABRUPT WARMING EVENTS OF THE LAST GLACIAL PERIOD

Xiao Yang

A dissertation submitted to the faculty of the University of North Carolina at Chapel Hill in partial fulfillment of the requirements for the degree of Doctor of Philosophy in the Department of Geological Sciences.

Chapel Hill
2016

Approved by:

Jose A. Rial

Jonathan M. Lees

Tamlin M. Pavelsky

J. Jason West

Donna M. Surge

ABSTRACT

Xiao Yang: Phase Synchronization Between Polar Climates: its Identification, Evolution, and Connection to the Abrupt Warming Events of the Last Glacial Period
(Under the direction of Jose A. Rial)

During the last glacial period, warming events with different characteristics occurred on each Polar Region. In the Greenland records, the warming episodes, are abrupt and strong. In contrast, the Antarctic events of the same age are gradual and mild. While it is generally accepted that these events have a one-to-one relationship, their exact linkage mechanism remains unknown.

In the following text, I have organized my research findings into three chapters, with each presenting a unique aspect of the polar climate relationship. In the first chapter, I associated the polar climates and their synchronization relation to the massive ice rafted detritus deposits (Heinrich events and IRD events) found across North Atlantic. Assuming the validity of the recent hypothesis of phase synchronization between polar records, I was able to develop indices that hindcast the timings of the Heinrich events. I then discussed the potential physical mechanisms that could connect the changes in the polar climates to the Heinrich events. In the second chapter, I conducted an inter-comparison study of all relevant published models, that seek to explain the polar climate connection, based on both their mathematical model properties, and their skills in reproducing actual records. Through the comparison, I demonstrated that the phase synchronization model exceeds the other two in its ability to reproduce actual records. While proposing the phase synchronization as a favorable framework, I also discussed the potential mechanism that integrates the phase synchronization and thermal bipolar seesaw models. After

established the phase synchronization as the most accurate and robust model, in my third and last chapter, I extracted the variations in the strength of the phase synchronization by calculating the windowed mean phase coherence between the polar ice core records. My results revealed that, with strong phase coherence during majority of the glacial period, instances of weak coherence did happen. More importantly, further analysis revealed a persistent insolation lead over the variations in phase coherence. This discovery provides new ways of interpreting not only the polar climate relationship itself, but also the origin of the glacial warming events.

to my parents
for their love and care

to Jackie
for the time past and the time yet to come

and to Xingyun
for I feel lucky to have you

ACKNOWLEDGEMENTS

I am thankful for the constant guidance and support from my advisor Jose Rial, without whom this work would never be possible. I am thankful to my committee members Tamlin Pavelsky, Jonathan Lees, Donna Surge and Jason West for their advice on my research and the revision of this work. This work presented here benefited greatly from conversations with my coauthor and colleague Elizabeth Reischmann, and many others from the Department of Geological Sciences at University of North Carolina at Chapel Hill. I would like to thank my parents, for their constant care and support through the years I pursue my training to be a scientist. I would also like to thank my wife Jackie and my son Xingyun for their accompanying and unconditional support.

TABLE OF CONTENTS

LIST OF TABLES

LIST OF FIGURES

CHAPTER 1: ON THE BIPOLAR ORIGIN OF HEINRICH EVENTS[1]

1.1. Introduction

A number of studies have suggested that the stable isotope temperature proxies from Greenland and Antarctica ice cores are not independent of each other [*Blunier et al.*, 1998; *Blunier and Brook*, 2001; *Knutti et al.*, 2004; *Steig*, 2006; *Barker et al.*, 2009, 2011]. For instance, the bipolar seesaw hypothesis [*Crowley*, 1992; *Broecker*, 1998; *Stocker and Johnsen*, 2003] states that since abrupt warming episodes in the North Atlantic occur at or near the beginning of gradual cooling in Antarctica, there must be a strong interaction of the polar climates through the meridional heat transport and North Atlantic deep water (NADW) production. EPICA Community Members [2006] then argued that, for most of the last glaciation, there is a 'one-to-one' assignment of each Antarctic warming with a corresponding stadial in the Greenland. While the classic bipolar seesaw proposes that the climate of the Earth's two poles are in anti-phase (180° or π), this has been proved to be insufficient in describing the entirety of the polar climate relationship [*Steig and Alley*, 2002; *Steig*, 2006]. Instead, the isotope records obtained from Greenland and Antarctica can be shown to be phase locked at 90° ($\pi/2$) for most of the last ice age, with the Antarctic climate variations leading that of Greenland's (for an overview of the polar phase synchronization idea, see [*Rial*, 2012; *Oh et al.*, 2014]; a short

[1] This chapter previously appeared as an article in the Geophysical Research Letters. Supplementary figures and texts have been integrated into the main text for this chapter. The original citation is as follows: Yang, X., J. A. Rial, and E. P. Reischmann (2014), On the bipolar origin of Heinrich events, *Geophysical Research Letters*, *41*(24), 9080–9086, doi:10.1002/2014gl062078.

introduction can also be found in Appendix 1 and Figure S1.1). The $\pi/2$ phase lock, while describing the climate relationship more precisely than the aforementioned 180° phase shift, still produces an apparent seesaw (coldest in the north corresponding to the peak warming in the south) such that the Antarctic warms while Greenland remains cold. The climatic consequences of this phase lock are important and discussed throughout this paper.

The $\pi/2$ phase lock and the interdependence of the polar climate time series have been interpreted as indications of polar synchronization [*Rial*, 2012], whereby the coupling created by the intervening ocean and atmosphere caused the climate variations of the Polar Regions to synchronize. The two polar climates behave like a pair of coupled nonlinear oscillators, mutually adjusting their (originally different) natural rhythms to a common frequency and constant $\pm\pi/2$ phase shift, which makes them an approximate Hilbert transform pair [*Bracewell*, 1986; *Rial*, 2012]. This relationship is correct within the uncertainties of both the methane-matched age model and AICC2012 age model (Figure S1.1; see the following section 1.2.1 for details on data and age models) and can thus be written as $g(t) \sim H[a(t)]$. Here $g(t)$ represents any of the $\delta^{18}O$ records from Greenland, $a(t)$ any of the $\delta^{18}O$ or deuterium records from Antarctica, and $H[\cdot]$ is the Hilbert transform operator. The inverse Hilbert transform is $a(t) \sim H^{-1}[g(t)]$. That is, taking any pair of age model matched ice core temperature proxy records from Greenland and Antarctica, one can be reproduced by performing the Hilbert transform (or inverse Hilbert transform) of the other [*Oh et al.*, 2014].

1.2. Data and methods

1.2.1. Data and unified age model

An accurate relative chronology is critical to study climate relationships from different ice cores, especially between bipolar ice core pairs. In order for records from the two Polar

Regions to be comparable, the age models for the stable isotope records used in this paper have been matched in one of two ways. Either they have been aligned via a Monte Carlo fitting approach based on the methane-matched BYRD and GRIP records (GRIP, NGRIP, and GISP2 from Greenland; BYRD, Dome C, VOSTOK, and FUJI from Antarctica; see details in age model matching in the Appendix 1 and figures therein) [*Blunier and Brook*, 2001; *Oh et al.*, 2014], or via the AICC2012 age model as published in Veres et al. [2013] (NGRIP from Greenland; Dome C, EDML, TALDICE, and VOSTOK from Antarctica). Both data sets led to essentially identical results (see Figure 1.1 for comparison between results from the two age models).

1.2.2. Methods: Calculation of the energy and inter-polar temperature gradient

To calculate the inter-polar gradient, we subtracted the Greenland records from the Antarctic ones using the age-matched records, and then added to the difference its own absolute value to rectify the results. Rectifying the difference between polar records shows only the difference when the Antarctic is relatively warmer than Greenland (Figure 1.2). Prior to subtraction, all records have been normalized (removed mean and divided by its standard deviation) under the assumption that temperature being proportional to the amount of $\delta^{18}O$, (see [*Johnsen et al.*, 1995]) then filtered using a Butterworth bandpass filter (with corner frequency at 0.0001 $year^{-1}$ and 0.001 $year^{-1}$) to eliminate the frequency components shorter than 1000 years or longer than 10000 years. We applied similar bandpass filter before estimating the energy density of the system (Figure 1.3). After filtering, the age-matched records, as well as records using the AICC2012 age model, were averaged for Antarctica in order to reduce local climate variations in individual record. Prior to calculating the sum of squares, a small constant has been added to the southern records to shift its baseline, the effect of which can be seen in Figure S1.4.

This is done since the baseline of neither record is known with precision, and a small value of a difference in baseline can improve the fit, as shown.

EMD (Empirical Mode Decomposition) was used to decompose the signal and verify if the linear Butterworth filter is applicable to the signal at hand. The EMD method, without assuming the character of the signal, utilizes extrema in the data to recursively decompose the data into several IMFs (Intrinsic Mode Function) that can be interpreted as the nonlinear components of the original data. Reconstruction via summing the IMFs of the frequency range interested provides a data adaptive decomposition (see Figure 1.2a).

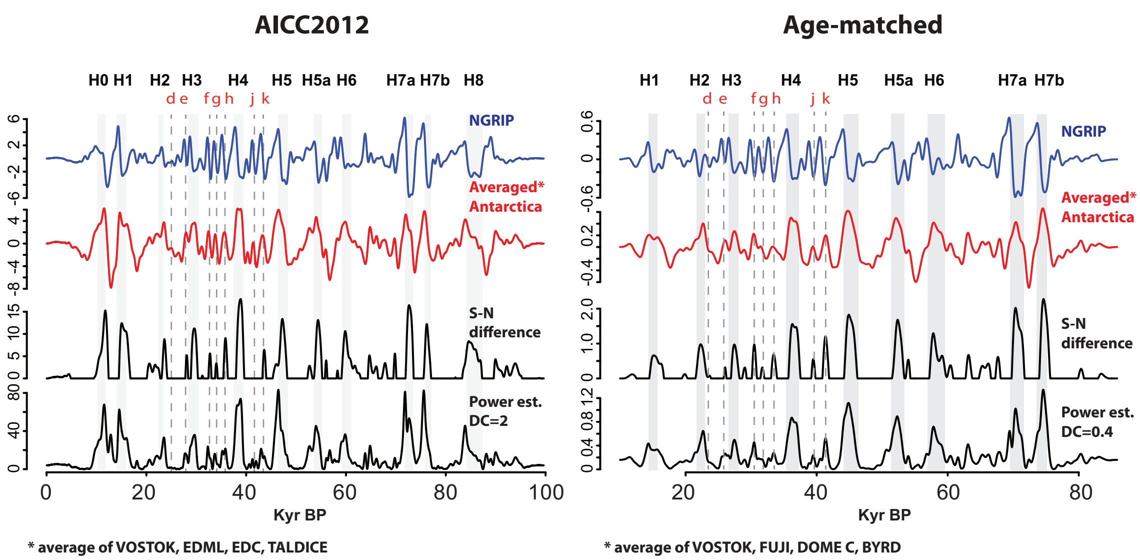

Figure 1.1. Temperature and power calculation for records based on AICC2012 age model [*Veres et al.*, 2013] as well as methane-age-matched records. The southern records from Antarctica have been averaged to reduce local climate variations. From top to bottom for both AICC2012 and age-matched calculation, the y-axis labels are: "Normalized $\delta^{18}O$-derived temperature", "Normalized $\delta^{18}O$-derived temperature", "Rectified normalized temperature gradient", and "Arrival of energy (arbitrary units)".

1.3. Results

1.3.1. Polar temperature differences

Regardless of the age model used, the $\pi/2$ phase shift aligns the coldest times of Greenland with the peak warming events of Antarctica. This causes the south to north polar temperature gradient to reach maxima of 10℃ to 15℃, coevals (within age uncertainty) with the H events (Figure 1.2) as described by Hemming [*Hemming*, 2004], as well as with the small pulses of IRDs described by Bond and Lotti [1995] that occur every 2-3 thousand years. It should be noted that the timings of both sets of events used in this paper are determined not by their absolute timing (which is uncertain) but rather is based on the previously established definition of H events that stipulates that these events happen when the Greenland climate reaches an extreme cold directly before an abrupt warming [*Bond et al.*, 1993; *Blunier and Brook*, 2001].

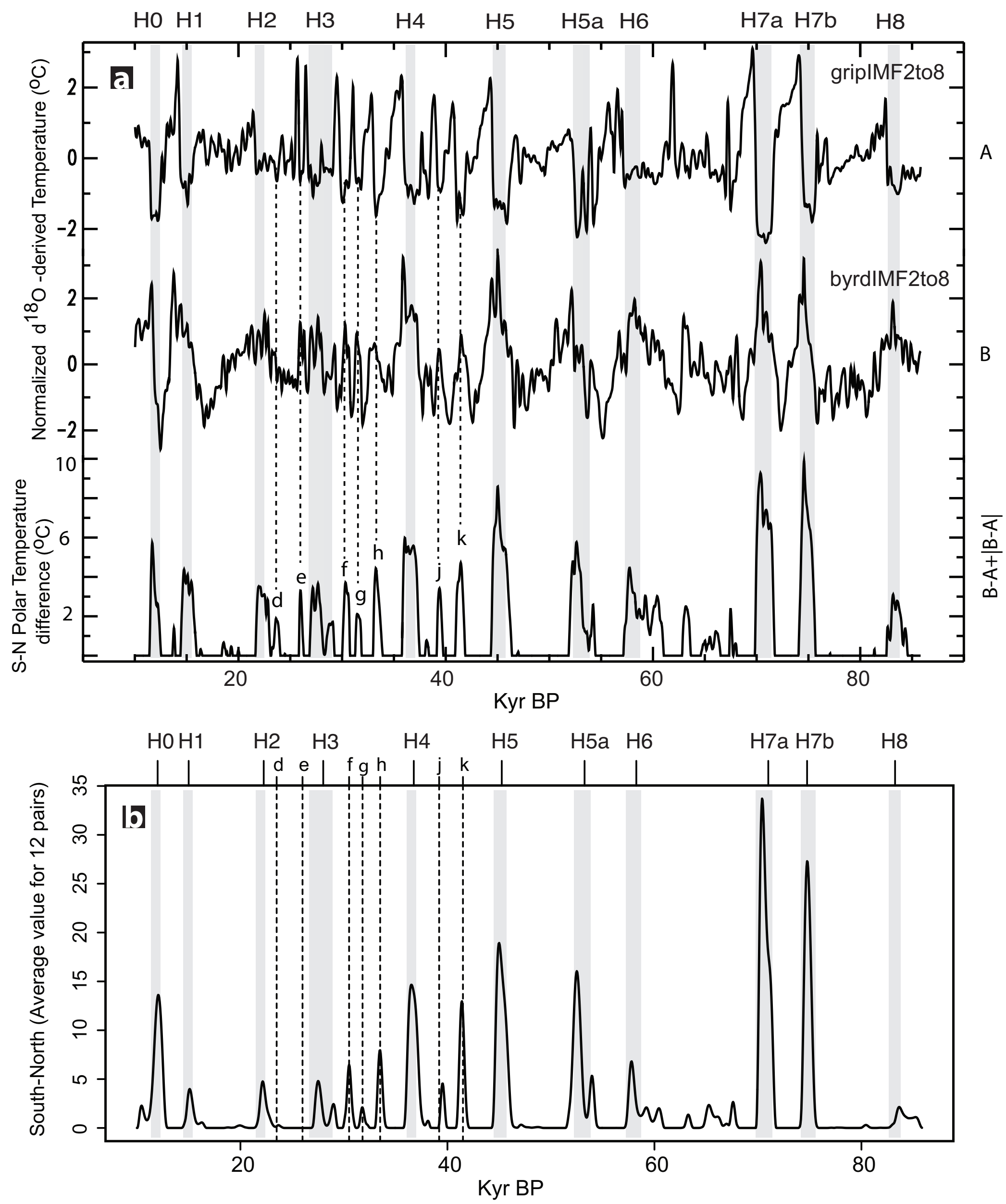

Figure 1.2. Polar climate S-N temperature gradient. **(a)** S-N temperature gradient from methane-matched, reconstructed time series GRIP and BYRD compared to the timing of the H events (vertical grey bars, see main text for detail) [*Bond and Lotti*, 1995; *Rashid et al.*, 2003; *Rasmussen et al.*, 2003; *Hemming*, 2004]. The timing of H events and even the timing of minor IRDs (labeled d-k) coincide with times at which the south to north temperature difference is the greatest, as seen in the bottom panel. Intrinsic Mode Functions 2 through 8 were extracted to bandpass-filter the records [*Huang et al.*, 1998]. The S-N temperature difference (B-A) is rectified. (**b)** S-N temperature differences for all 12 combinations of polar climate time series pairs (three from Greenland, four from Antarctica) with methane based Monte Carlo-matched age model.

H events are most commonly characterized by massive iceberg discharges of the northern ice sheets carrying coarse sediment to the open sea, occurring near the end of periods of extremely cold climate as recorded in Greenland's ice core records. Their influence beyond the region remains uncertain, as do the mechanisms that might trigger these icebergs releases. In most of the literature, the H events are regarded as uniquely Northern Hemisphere events [*MacAyeal*, 1993; *Bond and Lotti*, 1995; *Marshall and Clarke*, 1997; *Schulz et al.*, 2002; *MacAyeal et al.*, 2006; *Alvarez-Solas et al.*, 2010], though their full dynamic history remains incomplete. However, some recent publications have reported climatic events in the equatorial regions and the Southern Hemisphere that were coeval with the H events. For example, Jennerjahn et al. [2004] published evidence of the southward displacement of the ITCZ (Intertropical Convergence Zone) in the tropical Atlantic region, with increasing intensity of the northeast trade winds occurring during the H events enhancing the humidity and precipitation in the tropical South America. In addition, Whittaker et al. [2011] published work on speleothems from New Zealand's Hollywood cave (42°S) that shows abrupt shifts from cold and dry to wet and cool climates occurred at times that coincide with accepted ages of H events in the interval from 73 ka to 11 ka. Further, Sachs and Anderson [2005] suggest that H events may have been connected to sudden ocean productivity increases in the southeast Atlantic and southwest Pacific oceans.

1.3.2. Energy estimation of the polar climate variation

IRD layers in the North Atlantic are heuristically described as coming from detritus carried to the open ocean by 'armadas' of icebergs or by expanding sea ice but are seldom discussed in terms of their energy source, except for the binge-purge model [*MacAyeal*, 1993]. These layers include H events, which are large, anomalous processes that occur episodically (every 7 to 12 ka) and last a few hundred years [*Hemming*, 2004], which suggests the action of comparable anomalous, episodic releases of energy. The generally termed IRDs appear to involve much less energy, as will be shown later. The results shown in Figure 1.2 combined with the polar synchronization hypothesis suggests that a tentative measure of the power (energy rate-of-arrival) involved in the H events is possible.

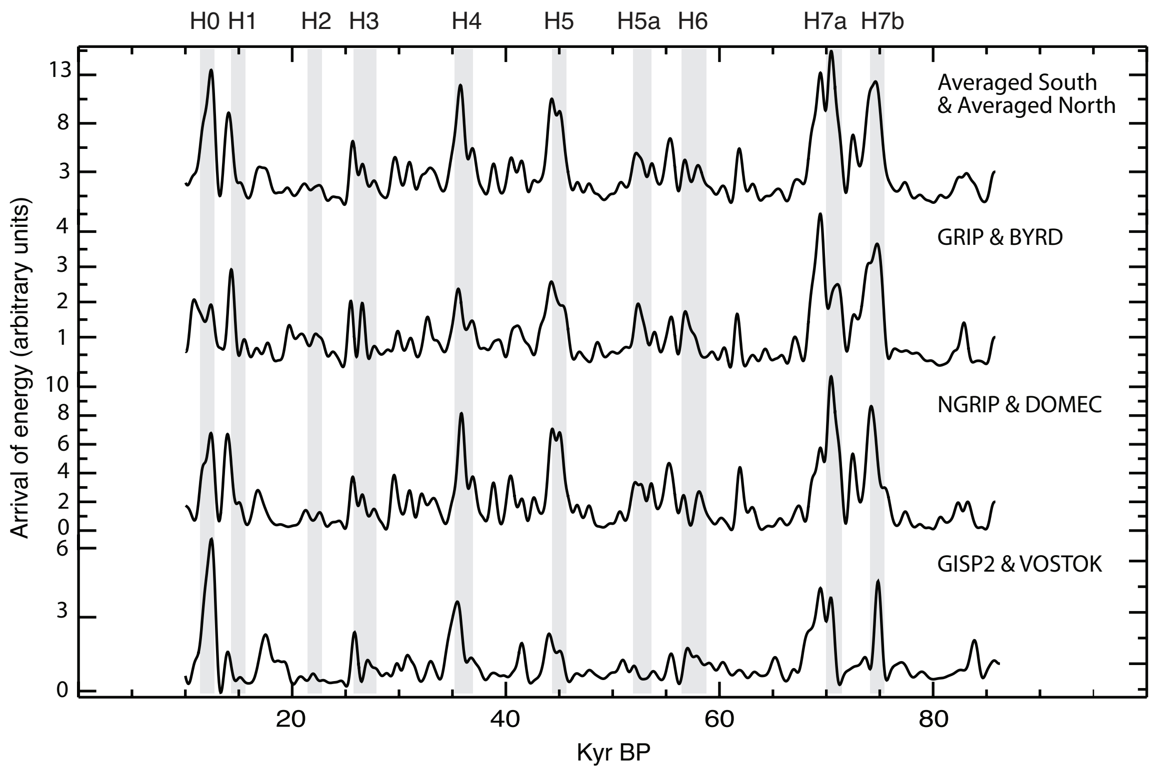

Figure 1.3. Rate of energy arrival (power) for four south-north isotope record pairs. From top to bottom the results are obtained by: all southern records, averaged and squared plus all northern records, averaged and squared; BYRD squared plus GRIP squared; Dome C squared plus NGRIP squared; and VOSTOK squared plus GISP2 squared. The sums, $|S(t)|^2 = a(t)^2 + g(t)^2$, appear as localized bursts (see text for details).

The persistent $\pi/2$ phase lock between the polar climate records allows the construction of an analytic function that consisting both climate signals. Having done so, the energy of the system that generates the analytic signal could potentially be estimated following Gabor's approach [*Gabor*, 1946]. We construct an analytic signal $s(t) \sim a(t) + ig(t)$, with magnitude $|s(t)| = \sqrt{a(t)^2 + g(t)^2}$, and total energy given by $E = \int_{-\infty}^{\infty} |s(t)|^2 dt$ (with $a(t)$ and $g(t)$ the same as defined in the introduction session). Thus, the instantaneous power of $s(t)$ is given by $dE/dt = |s(t)|^2 \sim a(t)^2 + g(t)^2$. This quantity is plotted in Figure 1.3 (see also Figure 1.1). Heyser [1971] showed experimentally, through the use of sound signals, that the square of the magnitude of an analytic signal (AS) is proportional to the instantaneous rate-of-arrival of the total energy of the real signal. By itself, the square of the original signal, say $|a(t)|^2$, would be proportional to the rate-of-arrival of just one of the components of the energy, and can thus be zero when any component of energy (kinetic or potential) vanishes. In contrast, the square of the magnitude of an AS would be zero only at those times when the total (kinetic plus potential) energy is zero. Notice that, in Figure 1.3, the energy minimum is near zero and that the smaller IRDs do not show as clearly as in the case of polar temperature gradient (Figure 1.2).

The estimated power from the function $|s(t)|^2 \sim a(t)^2 + g(t)^2$ produces episodic, pulse-like energy peaks that arrive at the times of the strong H events but at nearly no other time. This is a justifiable power estimate for the polar system considered because the stable isotope proxies represent not a single, identifiable climate variable, but the amplitude fluctuation of a function of some climate variables, and they are usually assumed to be linear or weakly nonlinear functions of regional or hemispheric temperature [*Johnsen et al.*, 1995]. Hence, the power estimates in Figure 1.3 can be used as a proxy of the total energy flux of the pole-to-pole climate oscillation.

1.4. Discussion

The results shown in Figure 1.2 and Figure 1.3 strongly suggest that the occurrence of H events is tied to the coupled climate oscillations of the poles, instead of being a process unique to the Northern Hemisphere or processes happening separately in both hemispheres. Specifically, these figures show that the pulses in energy closely correlated with the H events, as well as with the maxima in the south-north (S-N) temperature gradient, suggesting a strong relationship between the combined polar records and these abrupt events. This bipolar origin of H events would explain why the isotope proxies from Greenland or Antarctica do not show the H events directly, but rather, upon combining the effects of the two polar signals the presence of H events is revealed.

This interaction between the polar climates predicts that the $\pi/2$ phase shift should cause a pulse-like peak of temperature gradient (which here is assumed to be proportional to the difference between the isotope records from two Polar Regions) based on the assumption that the isotope proxy is a nearly linear function of temperature [*Johnsen et al.*, 1995]) at the times of H5a, H7a, H7b, and H8 (Figure 1.2b), which were discovered more recently than the others [*Rashid et al.*, 2003; *Rasmussen et al.*, 2003]. That is, the polar temperature gradient produces a series of large, isolated pulse-like peaks at ~53, ~72, ~75, and ~83 ka in our results, where these events were eventually found (relative to timings of adjacent IRD events). Further, the timings of the smaller amplitude IRDs, identified by *Bond and Lotti* [1995] with the letters d-k, are coincident with relatively smaller peaks of S-N polar temperature gradient. (Note that the IRD layers a-c in the sediment cores have not been recorded in the ice core proxies, see [*Bond and Lotti*, 1995]). In the entire 100 ky record of the last ice age there is only one instance, at 63 - 65 ka BP, in which a maximum (albeit relatively small compared to all others) in temperature gradient does not coincide with a potential IRD or H event. Notice that only the (positive) S-N temperature gradient coincides with the IRDs, which is why the temperature gradient time series in Figure 1.2 is rectified.

Although the uncertainties in relative timing of events happened around H events leave open the possibility that maxima in polar temperature gradient are the result of the Atlantic Meridional Overturning Circulation (AMOC) reduction/shutdown after fresh water input from a H event, this does not exclude the potential contribution of the S-N polar temperature gradient to the North Atlantic subsurface warming in initially triggering the H events. Previous research reporting the subsurface warming in either Atlantic basin or mid-depth tropical/South Atlantic, at the time of reduced AMOC, has ascribed downward mixing of heat from the lower latitude as the heat source [*Rühlemann et al.*, 2004; *Shaffer et al.*, 2004; *Marcott et al.*, 2011]. However, it is likely that the heat accumulating in the Southern Ocean, which is reflected as warming trend in the Antarctic ice core records, at the times of the reduced south-to-north heat transport (reduced AMOC) contributed to the North Atlantic subsurface warming via warming the low latitude surface ocean. Northward heat transport from the South Atlantic is supported by the fact that the South Atlantic is the only ocean basin that transports heat equatorward through the subtropical gyre [*Talley*, 1999]. The key here is that peaks in either subsurface warming [*Alvarez-Solas et al.*, 2013] or in the polar temperature gradient (this paper) might not necessarily correspond to the start of the H events, instead these peaks might correspond to a complete shutdown of AMOC near the end of the H events. Upon the initial release of icebergs into the North Atlantic, melted fresh water further caps the AMOC (which might lead to the "Heinrich mode" or "off mode" of ocean circulation [*Rahmstorf*, 2002; *Clark et al.*, 2007]), promoting further warming in the subsurface water and increase in the S-N polar temperature gradient. The release of icebergs would then diminish when the condition of the ice sheet is no longer suitable for further calving.

In previous research, the H events have either been seen as the cause of the collapse of AMOC [*Broecker*, 1994, 2003; *Timmermann et al.*, 2005], or as a consequence of the AMOC shutdown [*Clark et al.*, 2007]. However, the relative timing of the North Atlantic subsurface warming, of the maxima in S-N polar temperature gradient, and of the H events may suggest an intervolved relationship that could allow both of the aforementioned arguments to be true. Instead of happening one after another, the H events and the reduction of AMOC may have evolved together. The initial mild reduction (may correspond to the "stadial mode" [*Rahmstorf*, 2002]) in AMOC observed at the early stage of each stadial contributes to the subsurface warming, with heat coming both from the south and from the reduction in ocean convection in the North Atlantic. When the conditions of both the ice sheets and the subsurface heat are optimal, the initial fresh water input occurs, which, through the aforementioned positive feedback [*Clark et al.*, 2007], leads to the massive iceberg release that characterizes an H event. At the same time, the massive fresh water input after the initial released may finally collapse the NADW formation and lead to the "off mode" of the AMOC, which is followed by maxima in both polar temperature gradient and subsurface warming.

Despite fresh water input [*Shakun et al.*, 2012] and the many other proposed mechanisms [*Ganopolski and Rahmstorf*, 2002; *Banderas et al.*, 2014] that may explain the AMOC slowdown at the interstadial-stadial transition, the ultimate pacemaker for these recurring polar temperature gradient pulses, as well as for the power pulses at the times of the H events, remains unknown [*Bond et al.*, 2001; *Clark et al.*, 2007]. However, it can be inferred from our study that such a pacemaker, if it exists, is unlikely to be a single, regional, recurring process. On the contrary, in a complex, phase-locked system as the polar climates system appears to be, distinguishing a pacemaker (or forcing) from the response is very challenging [*Clarke et al.*, 1999].

One of the challenges of modeling the H events is reproducing the phase-lock of the ice-climate coupling [*Clarke et al.*, 1999]. This can be explained via the results of our study, as the behavior of the ice sheets (exemplified by H events and IRDs events) does appear to be coupled with the polar climate synchronization through either polar temperature gradient or energy propagation along the Atlantic basin, either of which may contribute to the coupling of the polar climates. While the role of the S-N polar temperature gradient has been proposed above, the physical processes underlying the energy estimation (Figure 1.3) need further investigation. Despite the analogy between an acoustic signal and the polar climate's composite signal via the concept of analytic signal, the energy that is calculated here likely results from different mechanisms than those involved in the acoustic systems. That is, even though the energy maxima reflect nearly all H events, what the energy truly represents in the physical climate system is still unclear.

Under the hypothesis of polar synchronization, each polar climate subsystem potentially affects and is affected by the other, causing both to be nonlinearly transformed (their natural frequencies gradually changing until they lock with each other) by their interaction. It is possible that the polar climates were originally independent, even chaotic, before becoming connected, coupled, climatic oscillations via oceanic heat transfer, potentially channeled by the thermohaline circulation (THC). In order to validate our hypothesis of the bipolar origin of H events, it is important to investigate various paleoclimate records in the intermediate latitudes for traces of transmission of a polar climate signal (or the evidence of coupling). We have found that an organic carbon record from core GeoB3912-1b offshore northeastern Brazil [*Jennerjahn et* *al.*, 2004] correlates with the S-N polar temperature gradient with correlation coefficient as great as 0.8 for the last 67,000 years (see Figure S1.5). This result, if proved correct, will serve to confirm our hypothesis. However, a unified age model or a comprehensive assessment of age model differences is needed to confirm such correlation.

REFERENCES

1. Alvarez-Solas, J., S. Charbit, C. Ritz, D. Paillard, G. Ramstein, and C. Dumas (2010), Links between ocean temperature and iceberg discharge during Heinrich events, *Nat. Geosci.*, *3*(2), 122–126, doi:10.1038/ngeo752.

2. Alvarez-Solas, J., A. Robinson, M. Montoya, and C. Ritz (2013), Iceberg discharges of the last glacial period driven by oceanic circulation changes, *Proc. Natl. Acad. Sci.*, *110*(41), 16350–16354, doi:10.1073/pnas.1306622110.

3. Banderas, R., J. Alvarez-Solas, A. Robinson, and M. Montoya (2014), An interhemispheric mechanism for glacial abrupt climate change, *Clim. Dyn.*, 1–12, doi:10.1007/s00382-014-2211-8.

4. Barker, S., P. Diz, M. J. Vautravers, J. Pike, G. Knorr, I. R. Hall, and W. S. Broecker (2009), Interhemispheric Atlantic seesaw response during the last deglaciation, *Nature*, *457*(7233), 1097–1102, doi:10.1038/nature07770.

5. Barker, S., G. Knorr, R. L. Edwards, F. Parrenin, A. E. Putnam, L. C. Skinner, E. Wolff, and M. Ziegler (2011), 800,000 Years of Abrupt Climate Variability, *Science*, *334*(6054), 347–351, doi:10.1126/science.1203580.

6. Blunier, T., and E. J. Brook (2001), Timing of Millennial-Scale Climate Change in Antarctica and Greenland During the Last Glacial Period, *Science*, *291*(5501), 109–112, doi:10.1126/science.291.5501.109.

7. Blunier, T. et al. (1998), Asynchrony of Antarctic and Greenland climate change during the last glacial period, *Nature*, *394*(6695), 739–743, doi:10.1038/29447.

8. Bond, G., W. Broecker, S. Johnsen, and J. McManus (1993), Correlations between climate records from North Atlantic sediments and Greenland ice, *Nature*.

9. Bond, G., B. Kromer, J. Beer, R. Muscheler, M. N. Evans, W. Showers, S. Hoffmann, R. Lotti-Bond, I. Hajdas, and G. Bonani (2001), Persistent Solar Influence on North Atlantic Climate During the Holocene, *Science*, *294*(5549), 2130–2136, doi:10.1126/science.1065680.

10. Bond, G. C., and R. Lotti (1995), Iceberg Discharges into the North Atlantic on Millennial Time Scales During the Last Glaciation, *Science*, *267*(5200), 1005–1010, doi:10.1126/science.267.5200.1005.

11. Bracewell, R. N. (1986), *The Fourier transform and its applications*, McGraw-Hill New York.

12. Broecker, W. S. (1994), Massive iceberg discharges as triggers for global climate change, *Nature*, *372*(6505), 421–424, doi:10.1038/372421a0.

13. Broecker, W. S. (1998), Paleocean circulation during the Last Deglaciation: A bipolar seesaw?, *Paleoceanography*, *13*(2), 119–121, doi:10.1029/97PA03707.

14. Broecker, W. S. (2003), Does the Trigger for Abrupt Climate Change Reside in the Ocean or in the Atmosphere?, *Science*, *300*(5625), 1519–1522.

15. Clarke, G. K. C., S. J. Marshall, C. Hillaire-Marcel, G. Bilodeau, and C. Veiga-Pires (1999), A Glaciological perspective on Heinrich events, in *Geophysical Monograph Series*, vol. 112, edited by U. Clark, S. Webb, and D. Keigwin, pp. 243–262, American Geophysical Union, Washington, D. C.

16. Clark, P. U., S. W. Hostetler, N. G. Pisias, A. Schmittner, and K. J. Meissner (2007), Mechanisms for an ~7-Kyr Climate and Sea-Level Oscillation During Marine Isotope Stage 3, in *Ocean Circulation: Mechanisms and Impacts—Past and Future Changes of Meridional Overturning*, edited by A. Schmittner, J. C. H. Chiang, and S. R. Hemming, pp. 209–246, American Geophysical Union.

17. Crowley, T. J. (1992), North Atlantic Deep Water cools the southern hemisphere, *Paleoceanography*, *7*(4), 489–497, doi:10.1029/92PA01058.

18. EPICA Community Members (2006), One-to-one coupling of glacial climate variability in Greenland and Antarctica, *Nature*, *444*(7116), 195–198, doi:10.1038/nature05301.

19. Gabor, D. (1946), Theory of communication. Part 1: The analysis of information, *J. Inst. Electr. Eng. - Part III Radio Commun. Eng.*, *93*(26), 429–441, doi:10.1049/ji-3-2.1946.0074.

20. Ganopolski, A., and S. Rahmstorf (2002), Abrupt Glacial Climate Changes due to Stochastic Resonance, *Phys. Rev. Lett.*, *88*(3), 038501, doi:10.1103/PhysRevLett.88.038501.

21. Hemming, S. R. (2004), Heinrich events: Massive late Pleistocene detritus layers of the North Atlantic and their global climate imprint, *Rev. Geophys.*, *42*(1), RG1005, doi:10.1029/2003RG000128.

22. Heyser, R. C. (1971), Determination of Loudspeaker Signal Arrival Times: Part 2, *J. Audio Eng. Soc.*, *19*(10), 829–834.

23. Huang, N. E., Z. Shen, S. R. Long, M. C. Wu, H. H. Shih, Q. Zheng, N.-C. Yen, C. C. Tung, and H. H. Liu (1998), The empirical mode decomposition and the Hilbert spectrum for nonlinear and non-stationary time series analysis, *Proc. R. Soc. Lond. Ser. Math. Phys. Eng. Sci.*, *454*(1971), 903–995, doi:10.1098/rspa.1998.0193.

24. Jennerjahn, T. C., V. Ittekkot, H. W. Arz, H. Behling, J. Pätzold, and G. Wefer (2004), Asynchronous Terrestrial and Marine Signals of Climate Change During Heinrich Events, *Science*, *306*(5705), 2236–2239, doi:10.1126/science.1102490.

25. Johnsen, S. J., D. Dahl-Jensen, W. Dansgaard, and N. Gundestrup (1995), Greenland paleotemperatures derived from GRIP borehole temperature and ice core isotope profiles, *Tellus*, *47B*, 624–629.

26. Knutti, R., J. Flückiger, T. F. Stocker, and A. Timmermann (2004), Strong hemispheric coupling of glacial climate through freshwater discharge and ocean circulation, *Nature*, *430*(7002), 851–856, doi:10.1038/nature02786.

27. MacAyeal, D. R. (1993), Binge/purge oscillations of the Laurentide Ice Sheet as a cause of the North Atlantic's Heinrich events, *Paleoceanography*, *8*(6), 775–784, doi:10.1029/93PA02200.

28. MacAyeal, D. R. et al. (2006), Transoceanic wave propagation links iceberg calving margins of Antarctica with storms in tropics and Northern Hemisphere, *Geophys. Res. Lett.*, *33*(17), L17502, doi:10.1029/2006GL027235.

29. Marcott, S. A., P. U. Clark, L. Padman, G. P. Klinkhammer, S. R. Springer, Z. Liu, B. L. Otto-Bliesner, A. E. Carlson, A. Ungerer, and J. Padman (2011), Ice-shelf collapse from subsurface warming as a trigger for Heinrich events, *Proc. Natl. Acad. Sci.*, *108*(33), 13415–13419.

30. Marshall, S. J., and G. K. C. Clarke (1997), A continuum mixture model of ice stream thermomechanics in the Laurentide Ice Sheet 2. Application to the Hudson Strait Ice Stream, *J. Geophys. Res. Solid Earth*, *102*(B9), 20615–20637, doi:10.1029/97JB01189.

31. Oh, J., E. Reischmann, and J. A. Rial (2014), Polar synchronization and the synchronized climatic history of Greenland and Antarctica, *Quat. Sci. Rev.*, *83*, 129–142, doi:10.1016/j.quascirev.2013.10.025.

32. Rahmstorf, S. (2002), Ocean circulation and climate during the past 120,000 years, *Nature*, *419*(6903), 207–214, doi:10.1038/nature01090.

33. Rashid, H., R. Hesse, and D. J. W. Piper (2003), Evidence for an additional Heinrich event between H5 and H6 in the Labrador Sea, *Paleoceanography*, *18*(4), 1077, doi:10.1029/2003PA000913.

34. Rasmussen, T. L., D. W. Oppo, E. Thomsen, and S. J. Lehman (2003), Deep sea records from the southeast Labrador Sea: Ocean circulation changes and ice-rafting events during the last 160,000 years, *Paleoceanography*, *18*(1), 1018, doi:10.1029/2001PA000736.

35. Rial, J. A. (2012), Synchronization of polar climate variability over the last ice age: in search of simple rules at the heart of climate's complexity, *Am. J. Sci.*, *312*(4), 417–448, doi:10.2475/04.2012.02.

36. Rühlemann, C., S. Mulitza, G. Lohmann, A. Paul, M. Prange, and G. Wefer (2004), Intermediate depth warming in the tropical Atlantic related to weakened thermohaline circulation: Combining paleoclimate data and modeling results for the last deglaciation, *Paleoceanography*, *19*(1), PA1025, doi:10.1029/2003PA000948.

37. Sachs, J. P., and R. F. Anderson (2005), Increased productivity in the subantarctic ocean during Heinrich events, *Nature*, *434*(7037), 1118–1121, doi:10.1038/nature03544.

38. Schulz, M., A. Paul, and A. Timmermann (2002), Relaxation oscillators in concert: A framework for climate change at millennial timescales during the late Pleistocene, *Geophys. Res. Lett.*, *29*(24), 2193, doi:10.1029/2002GL016144.

39. Shaffer, G., S. M. Olsen, and C. J. Bjerrum (2004), Ocean subsurface warming as a mechanism for coupling Dansgaard-Oeschger climate cycles and ice-rafting events, *Geophys. Res. Lett.*, *31*(24), L24202, doi:10.1029/2004GL020968.

40. Shakun, J. D., P. U. Clark, F. He, S. A. Marcott, A. C. Mix, Z. Liu, B. Otto-Bliesner, A. Schmittner, and E. Bard (2012), Global warming preceded by increasing carbon dioxide concentrations during the last deglaciation, *Nature*, *484*(7392), 49–54, doi:10.1038/nature10915.

41. Steig, E. J. (2006), Climate change: The south–north connection, *Nature*, *444*(7116), 152–153, doi:10.1038/444152a.

42. Steig, E. J., and R. B. Alley (2002), Phase relationships between Antarctic and Greenland climate records, *Ann. Glaciol.*, *35*(1), 451–456, doi:10.3189/172756402781817211.

43. Stocker, T. F., and S. J. Johnsen (2003), A minimum thermodynamic model for the bipolar seesaw, *Paleoceanography*, *18*(4), 1087, doi:10.1029/2003PA000920.

44. Talley, L. D. (1999), Some aspects of ocean heat transport by the shallow, intermediate and deep overturning Circulations, in *Mechanisms of Global Climate Change at Millennial Time Scales*, edited by P. U. Clark, R. S. Webb, and L. D. Keigwin, pp. 1–22, American Geophysical Union.

45. Timmermann, A., U. Krebs, F. Justino, H. Goosse, and T. Ivanochko (2005), Mechanisms for millennial-scale global synchronization during the last glacial period, *Paleoceanography*, *20*(4), PA4008, doi:10.1029/2004PA001090.

46. Veres, D. et al. (2013), The Antarctic ice core chronology (AICC2012): an optimized multi-parameter and multi-site dating approach for the last 120 thousand years, *Clim Past*, *9*(4), 1733–1748, doi:10.5194/cp-9-1733-2013.

47. Whittaker, T. E., C. H. Hendy, and J. C. Hellstrom (2011), Abrupt millennial-scale changes in intensity of Southern Hemisphere westerly winds during marine isotope stages 2–4, *Geology*, *39*(5), 455–458, doi:10.1130/G31827.1.

48. Wunsch, C. (2010), Towards understanding the Paleocean, *Quat. Sci. Rev.*, *29*(17–18), 1960–1967, doi:10.1016/j.quascirev.2010.05.020.

CHAPTER 2: POLAR CLIMATE TELECONNECTION OF THE LAST GLACIAL PERIOD: A MODEL INTER-COMPARISON STUDY[2]

2.1. Introduction

2.1.1. Polar climate teleconnection

Since ice core chronology matching techniques became available, the relationship between polar climates has been of great interest to the paleoclimate community [*Bender*, 1994; *Blunier et al.*, 1998; *Blunier and Brook*, 2001]. Although most studies agree on a one-to-one occurrence of warming events during the last glacial period [*Schmittner et al.*, 2003; *Blunier and Brook*, 2001; *EPICA members*, 2006], the difference in timing and especially in relative phase of these warming events inspired great interests in investigating the mechanism that connects the climates of the Earth's Polar Regions. In most paleoclimate studies, data are scarce and limited in resolution, thus models have been extensively used to gain information from data and to help bound the possible speculations on the mechanism. GCM-based experiments have drawn a close relationship between the bipolar teleconnection and the changes in AMOC (Atlantic Meridional Overturning Circulation) strength [*Clark et al.*, 2007; *Marcott et al.*, 2011]. Because of the complexity of the GCMs, it is difficult if not impossible to extract the major underlying physics responsible for the teleconnection. On the other end of the spectrum, conceptual models, with fewer parameters, are ideal in testing the connection mechanism, guiding the interpretation of climate records and informing the GCM experiments.

---

[2] This chapter in under review in the Planetary and Global Change. The original citation is: Yang, X. and J. A. Rial (2016), Polar Climate Teleconnection of the Last Glacial Period: A Model Inter-Comparison Study, *Global and Planetary Change.*

Multiple conceptual models have been proposed in the literature based on either the numeric relationship of the polar climate records or their own assumed underlying mechanism of polar climate teleconnection [*Schmittner et al.*, 2003; *Stocker and Johnsen et al.*, 2003; *Rial*, 2012]. However, as will be detailed later, previous model studies have used different data pre-treatments, and mostly focused on a single direction of record reconstruction. A comprehensive analysis and comparison of the skills of these conceptual models and the models' robustness against parameter change could provide vital information in guiding future climate reconstruction work and improve our understanding of coupling mechanism between polar climates. Furthermore, extending the Greenland climate record beyond the length of its ice core record has been of great interest and all the climate models analyzed here have been used for this purpose [*Siddall et al.*, 2006; *Barker et al.*, 2011; *Oh et al.*, 2014]. However, this practice was discouraged by recent discoveries from high resolution climate records, that the Greenland climate record could be decoupled from the rest of the polar climate system possibly due to the extended sea ice formation during some of the lengthened Greenland stadial [*Capron et al.*, 2010; *Landais et al.*, 2015]. Even though current conceptual models all assume a persistent and constant polar climate teleconnection, a comprehensive inter-comparison study of these models, as presented here, will lay the foundation for future investigation of the evolution of the polar climate coupling.

2.1.2. Models

The three models studied here can be briefly described as follows: 1) the Thermal Bipolar Seesaw model (TBS) [*Stocker and Johnsen*, 2003], which was built upon the canonical bipolar seesaw concept [*Crowley*, 1992], included the Southern Ocean as a heat buffer, integrating the heat propagating from the North Atlantic to the Antarctic, until it was recorded in the ice core; 2)

An alternative to the TBS was proposed by Rial [2012], who proposes that a phase synchronization (PhaseSync) was at play between polar climate oscillations, with the coupling being the energy transfer through intervening ocean and atmosphere; 3) The Integration/Differentiation model (I/D), the idea of which predates both the TBS and the PhaseSync but is still in active use [*Barker et al.*, 2011], and uses the simple mathematical transform in its name to relate the polar records. These conceptual models, after being verified by the existing records, have also been used to obtained the first order approximation of Greenland climate history beyond the extend of its ice core record [for example, see *Siddall et al.*, 2006; *Barker et al.*, 2011; *Oh et al.*, 2014].

In chronological order, the I/D model was the first conceptual model proposed that accounts for the difference in signal shapes between polar records. It was proposed when it became clear that a simple, linear cross-correlation was unable to capture the different signal shapes between polar records (which also means that a simple lead-lag relationship fails to describe the polar climate connection) [see the discussion in *Schmittner et al.*, 2003; *Huybers*, 2004; and *Schmittner et al.*, 2004]. The I/D model states that, with proper trend removal and amplitude adjustments, integrating Greenland's ice core temperature record or differentiating the Antarctic temperature record closely reproduces that of the other pole. This idea was revisited in [*Rial*, 2012], in which it was compared to the idea of phase synchronization. And a numeric differentiation was used to reconstruct an 800 kilo-year (kyr) millennial scale Greenland climate variation [*Barker et al.*, 2011].

Next, the TBS model [*Stocker and Johnsen*, 2003, see also *Stocker*, 2011] was proposed as an extension to the well-known bipolar seesaw model [*Crowley*, 1992]. In the original bipolar seesaw publication, the seesaw behavior was defined as an inverse temperature relationship between the polar regions [*Crowley*, 1992]. Conversely, the updated TBS model describes the Southern Ocean as a heat reservoir regulating the climate connection between the South Atlantic and the Antarctic. Based on this assumption, Stocker and Johnsen [2003] proposed that the Antarctic temperature variation can be reproduced from the convolution of the Greenland record with an exponential decay term that represents the damping effect of the Southern Ocean. Through trial and error, Stocker and Johnsen determined the characteristic time for the Southern Ocean was ~1120 years, which was consistent in orders of magnitude with that estimated from climate modeling work. Later, Siddall et al. [2006] applied the inverse of the TBS model to reconstruct Greenland climate history based on the longer Antarctic record.

More recently, Rial [2012] investigated the phase relationship between the methane-matched polar isotope records and proposed that the polar climate records have been in a state of phase synchronization for the last glacial period. While a relatively new idea in interpreting paleoclimate records, phase synchronization is a well-known communication mechanism between pairs of nonlinear oscillators or among a network of oscillators [*Pikovsky et al.*, 2001; see also Figure. S2.1 for a simple illustration of phase shift]. The phase synchronization as described above is reminiscent of Christiaan Huygens' famous description of the synchronization of two pendulum clocks (analogous to the two polar climates) loosely coupled by minute elastic strain signals (climate signals) sent along the wooden beam (atmosphere and ocean in the Atlantic basin) on which both hung [*Huygens*, 1986; *Pikovsky et al.*, 2001]. In fact, modern models of Huygens' clocks that share the same frequency band show that the phase lock between them can be $\pi/2$ for a wide range of weak to moderate coupling (beam stiffness) [*Fradkov and Andrievsky*, 2007]. According to the hypothesis by Rial [2012], the polar records from Greenland and Antarctica are phase locked on the millennial scale with a constant phase difference of $\pi/2$

for most of the last glacial period, which is a strong evidence of synchronization. This phase difference also explains the difference in signal shapes between the polar records.

The polar climate teleconnection investigated in this study depends heavily on the frequency band chosen [*Roe and Steig*, 2004]. Before applying the models, the polar records were routinely filtered to isolate the millennial scale frequencies. Furthermore, it is unknown whether or to what degree the changes in data pre-treatment would affect the final skills of the model. As summarized in Table 2.1, different studies have used different highpass/lowpass filters with different corner frequencies (see HP filter and LP filter columns) to isolate the millennial scale climate variations. Since each model was optimized in its original publication, it is likely that different models will require input with different frequency content to achieve optimized skills.

Direction	Model type	HP filter	LP filter	Reference	Remarks
$\boldsymbol{G \rightarrow A}$	I/D	10 ky	NA	Roe & Steig, 2004	
	TBS	8 ky	NA	Stocker & Johnsen, 2003	No mention of LP filter
	PhaseSync + VDP	~10 ky	~10 ky	Oh et al., 2014	EMD, SSA, and linear filter used
$\boldsymbol{A \rightarrow G}$	iI/D	MW: 7 ky	MW: 700 yr	Barker et al., 2011	MW: moving average window width
	iTBS	8 ky	1 ky	Siddall et al., 2006	Gaussian filter used

Table 2.1. Summary of types of filters and their parameters used in data pre-treatment for the conceptual models discussed in this study. EMD: empirical mode decomposition; SSA: singular spectrum analysis; MW: moving window average; LP: lowpass filter; VDP: Van der Pol oscillator. $G \rightarrow A$: reconstruction of Antarctic record based on that of the Greenland; $A \rightarrow G$: the reverse.

In addition to differences in data pre-treatment, all these models have been inverted to reproduce the records of another pole (the inverted models are denoted by prefixing "i" to their model names). Individual studies on these models often focused on reproducing the climate record for one of the two poles, with no unified test on the modeling skills when reproducing both poles simultaneously. As invertible climate models that represent the two-way communication of the polar climate system, it is reasonable to expect comparable (or symmetric) skills between reproducing Greenland and Antarctica record. However, there is no existing study that conducted this "two-way" test.

In view of the above questions, in the following work, we first summarize the filter property of each model by extracting their impulse responses, which, in the case of a linear time-invariant system, should fully describe the system's response to any input. Then we demonstrate and compare the models' ability to reproduce each polar climate record based on the record from the opposing pole. Lastly, we further test the sensitivity of these models against changing values of data pre-treatment parameters. Siddall et al. [2006] conducted similar test for the iTBS model, where they established that the skill of the iTBS depends on both the model parameter τ and the filter cutoff frequency σ. To test whether each model gives comparable skills for producing the records of north and south, the sensitivity analysis is carried out in both model directions.

2.2. Methods

2.2.1. Data

The data used in this study are a $\delta^{18}O$ proxy from the NGRIP ice core (Greenland) and a δD proxy from the EDC ice core (Antarctica). Both have been dated with the latest AICC2012 chronology [*Veres et al.*, 2013]. Previous modeling practices were based on different north-south matched chronologies, which may affect the comparison between the models. Here, we eliminate such effect from chronology differences by choosing AICC2012 as the proxy chronology, which is considered by most to have the least uncertainty for cross-polar record comparison [*Landais et al.*, 2015].

2.2.2. Data pre-treatment

Past polar climate ice core records exhibit a rich spectrum of oscillatory behaviors, from those in the Milankovitch band to those on the millennial, centennial, or weather-caused scale. The cross-pole one-to-one occurrences of the events studied here are of the millennial scale. Thus, before applying the model, the records were normally filtered to isolate the corresponding frequency band. To achieve this, we applied a 4^{th} order bandpass Butterworth filter with cutoff frequency from $1/8000$ to $1/800$ yr^{-1}. This effectively suppresses both the direct influence from the long Milankovitch-scale trend and the high frequency weather-like signal. The filtered records were then normalized, via division by its own standard deviation after mean removal, and tapered to reduce the end effect from the filtering process.

2.2.3. Transfer functions, convolution, and model characteristics

The I/D, TBS, and PhaseSync models were presented in their time domain forms in their original publications (see Appendix 1 for the original model equations), which means that one can implement the model via using polar climate records as the inputs for their respective formulas. While the time domain model formulas make implementation straight-forward, the filtering effects of each model are more obvious in their frequency domain representations. As the abrupt climate change events have oscillatory behaviors of various scales, it is beneficial to inspect how similar events of different periodicities are affected by each model. One method of doing so is through an inspection of the transfer function of each model. By definition, a transfer function is the response of a system after an impulse signal was given as the input. In the case of the conceptual polar climate models, the transfer function is the model output when a Dirac function was input to the model. The transfer function is an intrinsic property of each model and is independent of the model input [*Oppenheim et al.*, 1996]. Once obtained, any model response $y(t)$ can be calculated by convolving the model input $x(t)$ with its transfer function $h(t)$.

$$y(t) = x(t) \otimes h(t)$$

where the $\otimes$ denotes the convolution operation.

Once calculated, the transfer function of each model was Fourier transformed to obtain the amplitude and phase responses. The transfer functions and their frequency domain representations are summarized in Table 2.2 and Figure 2.1 for the Greenland to Antarctica direction. A detailed comparison of the model amplitude and phase responses and its implication will be presented in depth in the following Results section.

Model	Time domain	Frequency domain	Description
I/D	$-\frac{1}{\Delta t}$	$\frac{1}{j2\pi k\Delta f}$	
TBS	$-e^{-\frac{i\Delta t}{\tau}}$	$\frac{\tau}{1+j2\pi k\Delta f\tau}$	
PhaseSync	$\left(\frac{2}{N}\right)\sin\left(\frac{i\pi}{2}\right)^2\cot\left(\frac{i\pi}{N}\right)$	$-j\, sgn\left(\frac{N}{2}-k\right)\, sgn(k)$	N is even
	$(1/N)[\cot(i\pi/N)-\cos(i\pi)/\sin(\frac{i}{N}\pi)]$		N is odd

Table 2.2. Transfer functions for the conceptual models. For the time domain representation, i is the index number ranging from 1 to the length of the record N. For the frequency domain representation, j is the square root of -1 and k is the index of the frequency. See Figure 2.1 for visualization of the transfer functions, their amplitude and phase responses.

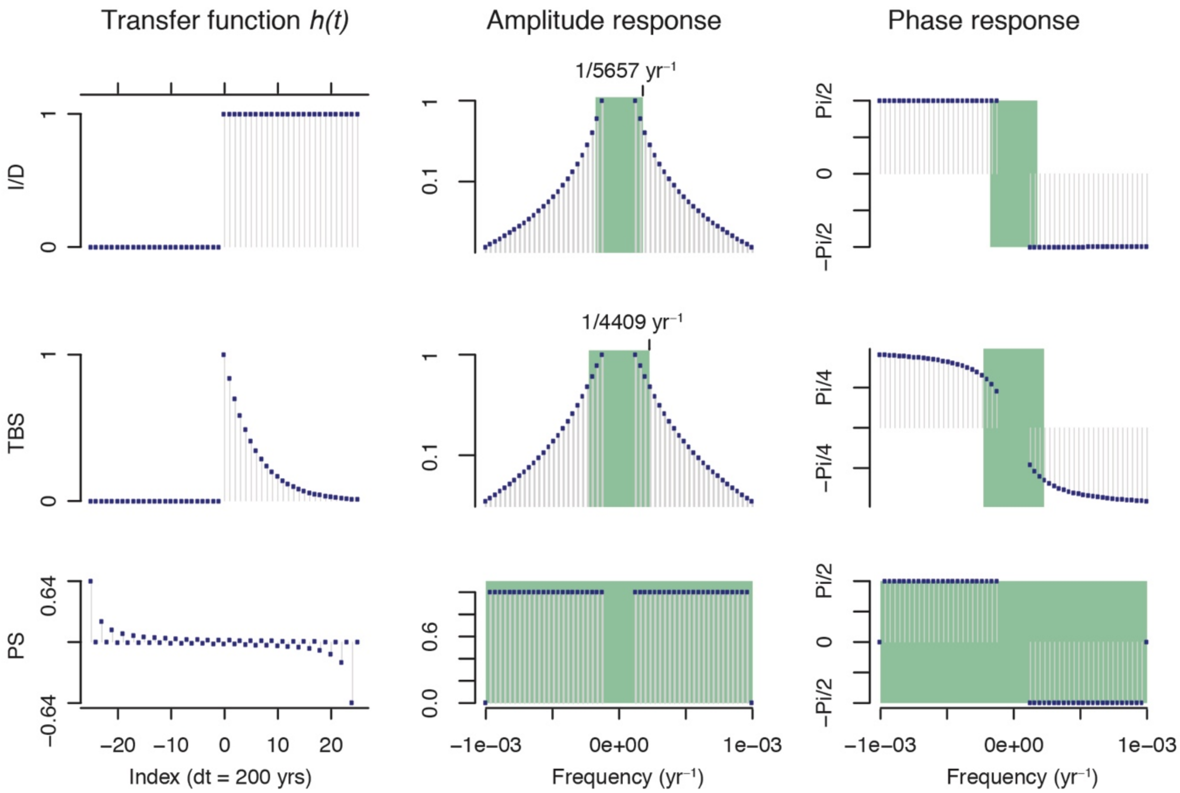

Figure 2.1. Model characteristics. *Left column*: time domain representations of the model transfer functions. $\tau = 1120$ years is used to calculate the transfer function for TBS model. *Middle column*: amplitude responses of the transfer functions. The green portion spans the passband of the amplitude responses and the values of the corner frequencies are shown for the I/D and TBS models. *Right column*: phase responses of the transfer functions. The I/D and PhaseSync models both have a $\pi/2$ phase response. Initial Butterworth filters has removed frequencies lower than $1/8000$ yr^{-1}, the effect of which is represented as the gap at the low frequencies of the amplitude and phase responses.

2.3. Results

2.3.1. Comparison of amplitude and phase responses

As revealed in Figure 2.1, both the I/D and TBS models intrinsically function as low-pass filters, which pass the low frequency part of the model input while suppressing the high frequency part. While the two models become identical when τ goes to infinity, when the τ is in the range of hundreds of years, theoretical cutoff frequencies of the two filters have one order of magnitude difference, such that the I/D model suppresses the high frequency further than the TBS model. However, the actual implementations of the I/D and TBS models yield almost identical results (see simulations in Figure 2.2a). This similarity is caused by removal of the low frequency portion of the record, where the two filters differ the most, in the data pre-treatment step that was meant to isolate the millennial frequencies. The effect from this initial filter is shown in Figure 2.1 as the gap at the low frequency region of the amplitude and phase responses, while the green rectangle represents the passing band of each model. The simulation in Figure 2.2a results from sequentially applying the Butterworth bandpass filter and the polar teleconnection models, showing their combined effect. This combined effect further reveals that the I/D and TBS models share very similar structure in their amplitude responses (see Figure 2.1 and Figure. S2.2). The results from the PhaseSync model, represented by Hilbert transformation, show that the model functions as an all pass operation that does not change the amplitude of any frequency. However, it does apply a $\pi/2$ phase shift to the model input, which, in this respect, is the same as the I/D model.

2.3.2. Modeling Antarctic record

With the tapered, normalized, and filtered NGRIP and EDC records, the implementation of each model was carried out by convolving a polar record with each transfer function. Then the model outputs are compared to the tapered, normalized, and filtered actual records by calculating the Pearson correlation coefficient between them. The model formulas and their inverted versions can be found in Appendix 2.

We first applied the models to simulate the Antarctic EDC record from that of Greenland's NGRIP (Figure 2.2a). The cross-correlation function (CCF) in Figure 2.2c shows that all three models yielded similar reconstructions, and they all closely reproduce the target Antarctic EDC record with maximum correlation values of 0.76, 0.73, 0.73 for the I/D, TBS, and the PhaseSync model respectively. The lags that correspond to maximum correlation in Figure 2.2c are less than 200 years and are well within the chronology uncertainties of the record. However, the actual EDC δD has distinctive structures that are not replicated by any of the models. For example, the actual record showed complex peak structures (see double/multiple peaks at 54, 39, and 15 kya in EDC in Figure 2.2a). None of the models investigated here were able to replicate these structures. These complex peak structures in the EDC record may result from local climate variations that were independent from the polar climate teleconnection.

2.3.3. Modeling Greenland record

The model skills differentiate between the PhaseSync and the other two models when reconstructing the Greenland climate from the EDC record (Figure 2.2b&d). CCF analysis reveals that reconstruction from the iPhaseSync model, with the maximum correlation value of 0.73, more closely simulates the NGRIP record than the reconstructions from either the iTBS (0.57) or the iI/D model (0.61). The outputs from the iI/D and iTBS models are similar to each other, but then comparing to the actual NGRIP record, they are not as accurate as the output from the PhaseSync model. The relative amplitudes of the short-duration warming events in marine isotope stage 3 (MIS3) are over-amplified for the iI/D and iTBS models when compared to the actual NGRIP record. Also, the lead-lag relations between model results and the target NGRIP record are consistent (Figure 2.2d), with the model results lagged behind the Greenland record by about 170 years on average (232 years for the iTBS model, 150 years for the iPhaseSync model, and 134 for the iI/D model). Even though this lag may be the consequence of systematic chronology uncertainty, it is consistent with the recent discovery based on WAIS-Divide ice core, which showed abrupt warmings in Greenland on average led those in the Antarctica by 218 ± 92 years [*Buizert et al.*, 2015].

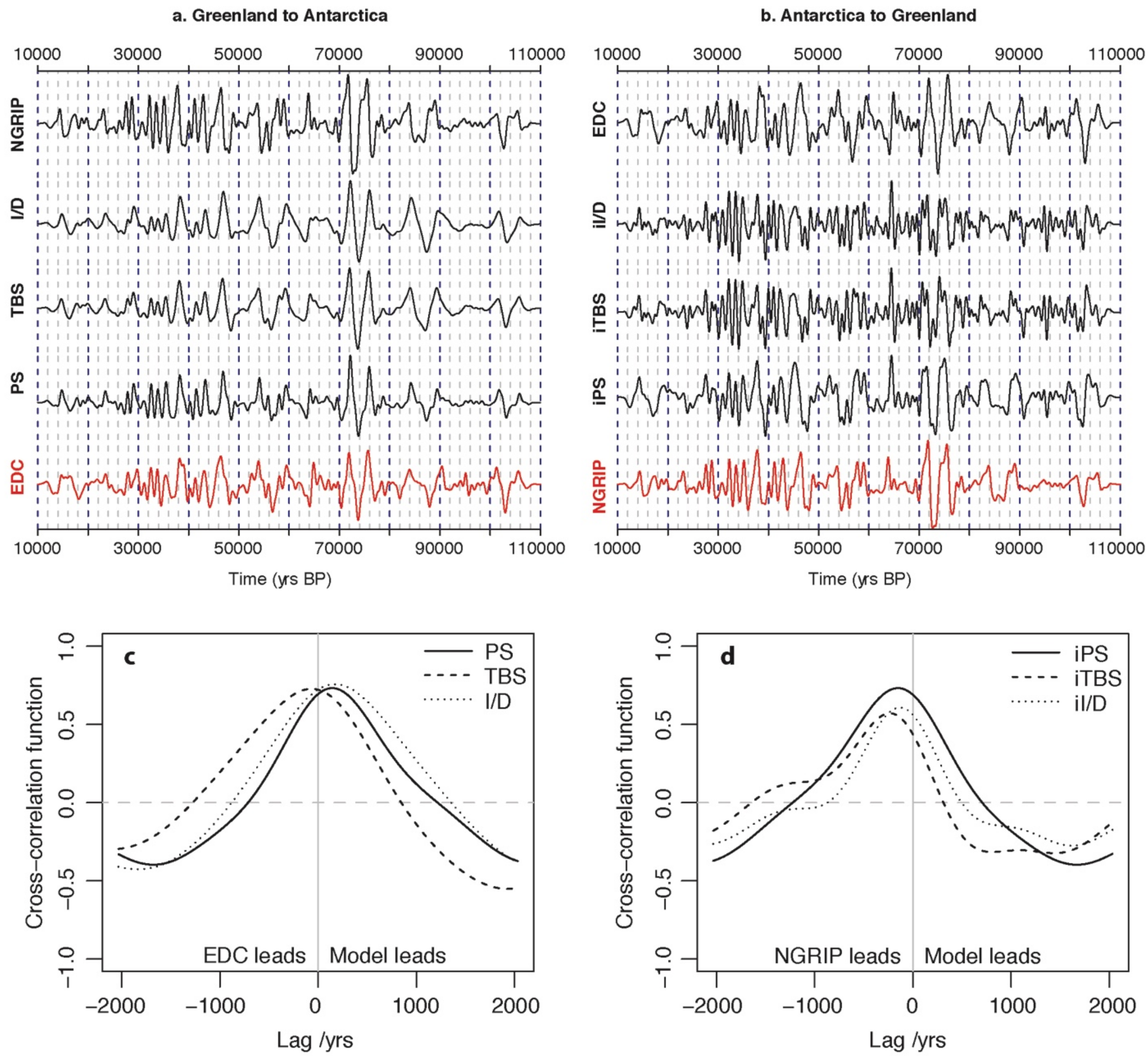

Figure 2.2. Modeling Greenland and Antarctica records. a. Simulation of the Antarctic EDC record based on the NGRIP record from Greenland. Both EDC and NGRIP have been band-pass filtered, normalized, and then tapered. The input NGRIP record is then convolved with each model transfer function. The results are labeled as their model names "I/D", "TBS", and "PhaseSync". The τ value was set to 1120 yrs for the TBS model [as in Stocker & Johnsen, 2003]. EDC ice core record (in red) is shown at the bottom as a reference for visual comparison. b. Simulation of the Greenland NGRIP record based on the EDC record from the Antarctic. Both EDC and NGRIP have been processed in the same way as in (a). Then the input EDC record is used to convolve with transfer functions from the inverse of the polar teleconnection models that are labeled as "iI/D", "iTBS", and "iPhaseSync". The NGRIP (in red) is shown at the bottom as a reference. c-d. cross-correlation functions between each of the model results and the target record (EDC in c and NGRIP in d).

2.3.4. Model skill and robustness against data pre-treatment

In order to estimate the skills of these models in reproducing the Antarctic record, we calculated the Pearson correlation coefficients between the simulations and the EDC δD record. As the result of the TBS model depends on the value of the τ parameter, we simulated the Antarctic record using different τ ranging from 0 to 6000 yrs and plotted the correlation as a function of τ (Figure 2.3a). The correlation coefficients for the other two models are also shown for comparison. The result shows that the skill of the TBS becomes less sensitive to the τ value beyond ~1000 yrs, suggesting one might need extra justification for choosing τ value in this range. In addition, the tendency of convergence between the TBS and I/D models can be observed from Figure 2.3a with increasing value of τ.

Unlike reproducing the Antarctic record, previous studies have shown that the skill of the iTBS model is very sensitive to the change of the smoothing parameter in the data pre-treatment stage, due to the tendency of the iTBS and iI/D models to amplify high frequency components. Here, this smoothing factor is controlled by the lowpass cutoff frequency of the Butterworth filter (denoted by σ). To determine the robustness of model skills against changes in this parameter, we have varied the value of σ in the interval between $1/3000$ to $1/200$ yrs^{-1} and plotted the corresponding model skills in Figure 2.3b for each inverted model. We also fixed the σ value at 1000 years (yrs) and calculated the skill of iTBS model with varying values of τ. The pair of values that corresponds to the maximum skill of the iTBS in Siddall et al. [2006] was $\sigma = 1000$ yrs and $\tau = 500$ yrs. However, since we are using a different data set with a different chronology (see [*Stocker and Johnsen*, 2003] for data used there), we do not expect to obtain the exact same optimal values. We are aware of the potential differences in modeling results that may be due to the differences in the chronologies used. Since we are using the same record pair and the same chronology consistently throughout this study, such effect is minimized.

The results shown in Figure 2.3b-c suggest that in order to choose the corner frequency of the low-pass filter σ, one has to compromise between model resolution and the noise-to-signal ratio. The higher the σ value, the higher frequency variations will be included in the input signal. This means that the models are more likely to be able to replicate the fine details of the abrupt northern climate variations. However, using a high value of σ leads to the model results being dominated by noise. This is especially the case for iI/D and iTBS models. In the extreme case of no low-pass filter used, the results of the iTBS and iI/D models are close to pure noise (see Figure. S2.3). We used $\sigma = 1/800$ yr^{-1} for the simulations in Figure 2.2b (a similar value to [Barker et al., 2011]'s $1/750$ yr^{-1}). It is worth noting that a proper low-pass filter will also increase the skill of the PhaseSync model. But such a filter is not necessary for the PhaseSync model to perform well (the correlation coefficient between the NGRIP record and the simulation from the PhaseSync model with no low-pass filter is about 0.5).

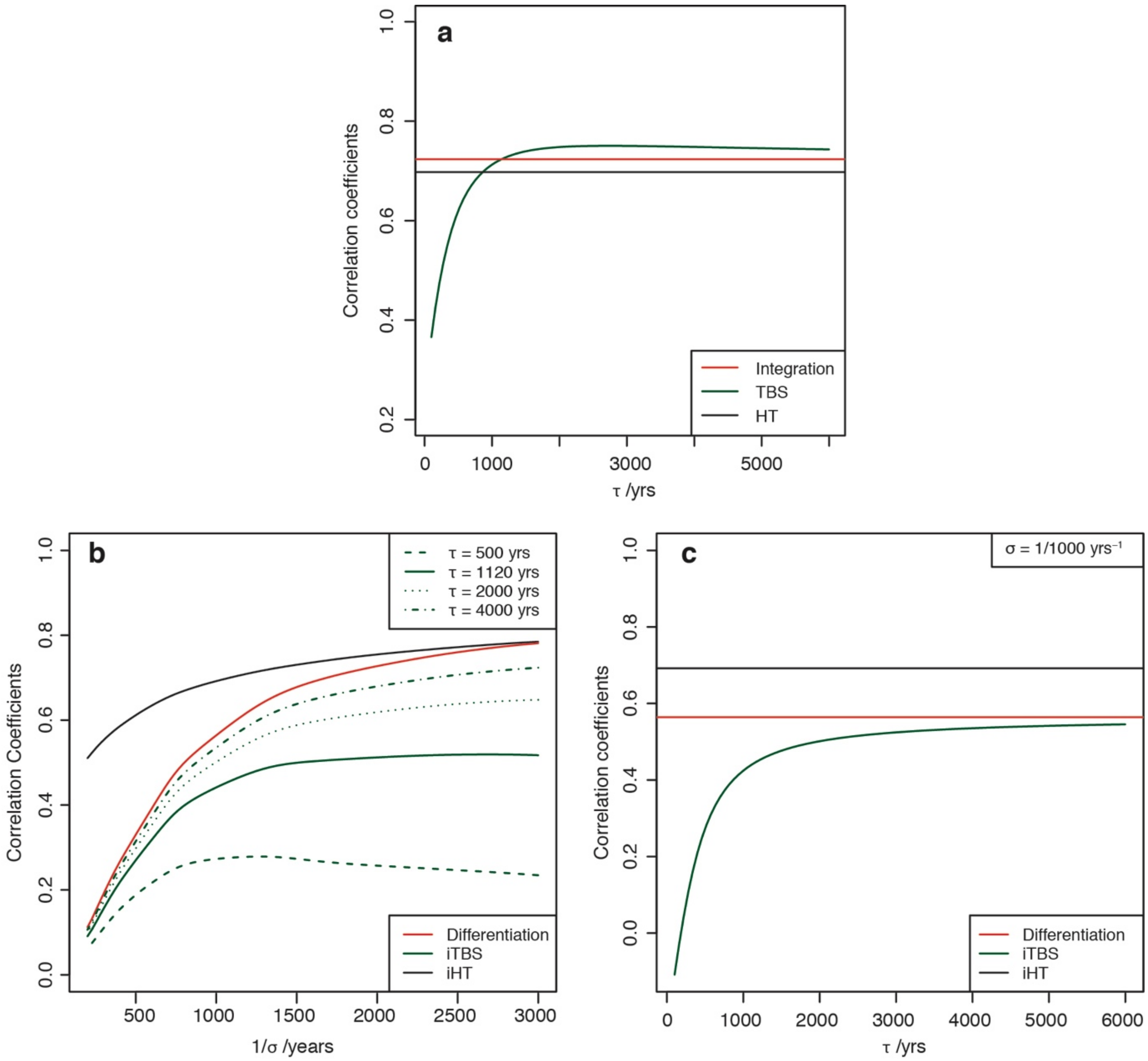

Figure 2.3. Model skills against change in data-pretreatment parameters. a. Model skills in reproducing the Antarctic record measured in the Pearson correlation coefficients between the simulations and the actual EDC record. The skill of the TBS model depends on the value of τ. b-c. Model skills represented by correlation coefficients between the simulations and the actual NGRIP record. b. The dependence of model skill on the corner frequency σ of the low-pass filter while fixing τ at four different values ranging from 500 to 6000 yrs. c. The dependence of model skill on the time constant τ from the iTBS model while fixing σ at $1/1000$ yr^{-1}. HT and iHT denote the phase synchronization model and its inverse.

So far, we have summarized the robustness of the model skills in reproducing the original record of a single pole. To conclude, with the same dataset and data pre-treatment, we have compiled the model skills in reproducing both polar records against changing value of σ (see Figure 2.4). As shown in the figure, the PhaseSync is the most robust of the three models, as its skill in reproducing both polar records stays the highest for almost all values of σ. Yet it yields comparable skills for reproducing the records from both poles (notice that the results from PhaseSync are close to the line of slope = 1). Conversely, the I/D and TBS models are slightly better at reproducing the Antarctic record than the PhaseSync model for some low values of σ, but their skills differ greatly in their ability to reproduce the Greenland records and their ability to reproduce the Antarctic records. Specifically, as can been seen from Figure 2.4, their skills in the Antarctica-to-Greenland direction are noticeably sensitive to changes in parameter σ in the range of $1/3000$ to $1/200$ yr^{-1}.

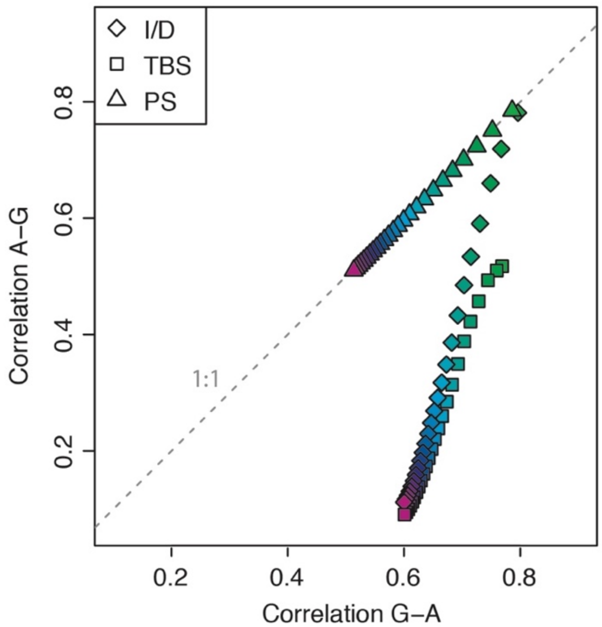

Figure 2.4. Model skills when taken into account both directions. The colors from green to purple represent corner frequency σ of the low-pass filter ranging from $1/3000$ to $1/200$ yr^{-1}.

2.4. Discussion

The models investigated in this study represent our current conceptual understanding of the teleconnection between the polar climates. Of the three models investigated, the I/D and TBS models share many numeric properties, which can be explained by the fact that the latter converges to the former model when its τ parameter approaches infinity. Both behave as low-pass/high-pass filters in the Greenland-to-Antarctica/Antarctica-to-Greenland directions, respectively. Furthermore, their skills are both asymmetric and sensitive to the inclusion of high frequency content in the model input (Figure 2.4). While the TBS and I/D models selectively suppress the high frequency content of the input (or the low frequency with their inverse), the PhaseSync model passes all the frequency content. Because of this property, the PhaseSync model is the most robust one against inclusion of noise or high frequency climate variations in the model input, requiring the least tuning of the data. And in contrast to I/D and TBS models, its skill is directionally symmetric (that is, comparable skills under the same data pre-treatment) in reproducing polar records.

Both the TBS and PhaseSync models were originally built upon assumptions of specific physical processes. The TBS model attributed the polar climates coupling to the heat transfer in the Atlantic Ocean. In its original form, Stocker and Johnsen [2003] derived the Antarctic temperature evolution as the result of heat transfer from the north, thus a north-to-south one-way coupling. In contrast, the phase synchronization model requires a bi-directional coupling between the polar climate oscillations. Although it does not inherently restrict the exact form of coupling, the intervening oceanic and atmospheric processes provide various potential mechanisms of coupling. A particular form of the polar climate coupling proposed by Rial [2012] was based on two coupled nonlinear Van der Pol oscillators originally conceived by

Saltzman [1982; 2002]. In this specific modeling setting, the polar climate oscillators, being coupled through the difference in the mean temperature of the ocean between the northern and southern hemispheres, is able to reproduce both the characteristics of polar records and their coupling. This provides a relationship between the poles that involves the mutual interaction between the two Polar Regions, an appealing mechanism based in well-known properties of nonlinear coupled synchronizing oscillators. As a possible signal pathway, the cross-pole, oceanic, heat transfer described in the TBS model could potentially contribute to the coupling of the polar climate oscillations.

In conclusion, polar teleconnection conceptual models not only provide a mathematical description of the relationship between ice core records, they also suggest potential physical coupling mechanisms. Here, we have analyzed the skills of three teleconnection models and discussed their underlying physical mechanisms. We found that the PhaseSync model outperforms the I/D and TBS models for a wide range of parameter values, accurately reproducing climate records from both poles. We introduced the merits of phase synchronization as a framework for the polar climate teleconnection and suggest that the oceanic heat transfer as described in the thermal bipolar seesaw conceptual model could be integrated into the synchronization framework as a mechanism of coupling between the polar climate oscillations. Future studies will try to establish the evolution of the coupling strength between the polar climates and utilize that information to assess reconstruction and extension of polar climate based on the conceptual models.

REFERENCES

1. Barker, S., G. Knorr, R. L. Edwards, F. Parrenin, A. E. Putnam, L. C. Skinner, E. W. Wolff, and M. Ziegler (2011), 800,000 years of abrupt climate variability, Science, 334(6054), 347–351, doi:10.1126/science.1203580.

2. Bender, M., T. Sowers, M.-L. Dickson, J. Orchardo, P. Grootes, P. A. Mayewski, and D. A. Meese (1994), Climate correlations between Greenland and Antarctica during the past 100,000 years, Nature, 372(6507), 663–666, doi:10.1038/372663a0.

3. Blunier, T. et al. (1998), Asynchrony of Antarctic and Greenland climate change during the last glacial period, Nature, 394(6695), 739–743, doi:10.1038/29447.

4. Blunier, T., and E. J. Brook (2001), Timing of millennial-scale climate change in Antarctica and Greenland during the last glacial period, 291(5501), 109–112, doi:10.1126/science.291.5501.109.

5. Buizert, C. et al. (2015), Precise interpolar phasing of abrupt climate change during the last ice age, *Nature*, *520*(7549), 661–U169, doi:10.1038/nature14401.

6. Capron, E., A. Landais, J. Chappellaz, A. Schilt, and D. Buiron (2010), Millennial and sub-millennial scale climatic variations recorded in polar ice cores over the last glacial period,, doi:10.1029/2003PA000920/full.

7. Clark, P. U., S. W. Hostetler, N. G. Pisias, A. Schmittner, and K. J. Meissner (2007), Mechanisms for an~ 7-kyr climate and sea-level oscillation during marine isotope stage 3, *Geophys. Monogr. Ser.*, *173*, 209–246, doi:10.1029/173GM15.

8. Crowley, T. J. (1992), North Atlantic Deep Water cools the southern hemisphere, Paleoceanography, 7(4), 489–497, doi:10.1029/92PA01058.

9. Fradkov, A. L., and B. Andrievsky (2007), Synchronization and phase relations in the motion of two-pendulum system, *International Journal of Non-Linear Mechanics*, *42*(6), 895–901, doi:10.1016/j.ijnonlinmec.2007.03.016.

10. Huybers, P. (2004), Comments on “Coupling of the hemispheres in observations and simulations of glacial climate change” by A. Schmittner, O.A. Saenko, and A.J. Weaver, Quaternary Science Reviews, 23(1-2), 207–210, doi:10.1016/j.quascirev.2003.08.001.

11. Huygens, C. (1986), *Christiaan Huygens' the pendulum clock, or, Geometrical demonstrations concerning the motion of pendula as applied to clocks*, Iowa State Pr.

12. Landais, A. et al. (2015), A review of the bipolar see–saw from synchronized and high resolution ice core water stable isotope records from Greenland and East Antarctica, *Quaternary Science Reviews*, *114*, 18–32, doi:10.1016/j.quascirev.2015.01.031.

13. Lisiecki, L. E., and M. E. Raymo (2009), Diachronous benthic δ18O responses during late Pleistocene terminations, *Paleoceanography*, *24*(3), doi:10.1029/2009PA001732.

14. Marcott, S. A. et al. (2011), Ice-shelf collapse from subsurface warming as a trigger for Heinrich events, *PNAS*, *108*(33), 13415–13419, doi:10.1073/pnas.1104772108.

15. Oh, J., E. Reischmann, and J. A. Rial (2014), Polar synchronization and the synchronized climatic history of Greenland and Antarctica, Quaternary Science Reviews, 83, 129–142, doi:10.1016/j.quascirev.2013.10.025.

16. Oppenheim, A. V., A. S. Willsky, and S. H. Nawab (1996), *Signals and Systems (2nd Ed.)*, Prentice-Hall, Inc., Upper Saddle River, NJ, USA.

17. Pikovsky, A., M. Rosenblum, and J. Kurths (2001), Synchronization. Cambridge Nonlinear Science Series 12.

18. Rial, J. A. (2012), Synchronization of polar climate variability over the last ice age: in search of simple rules at the heart of climate's complexity, Am J Sci, 312(4), 417–448, doi:10.2475/04.2012.02.

19. Roe, G. H., and E. J. Steig (2004), Characterization of Millennial-Scale Climate Variability, Journal of Climate, 17(10), 1929–1944, doi:10.1175/1520-0442(2004)017<1929:COMCV>2.0.CO;2.

20. Saltzman, B. (1982), Stochastically-driven climatic fluctuations in the sea-ice, ocean temperature, CO_2 feedback system, *Tellus*.

21. Saltzman, B. (2002), *Dynamical Paleoclimatology*, Academic Press.

22. Schmittner, A., O. A. Saenko, and A. J. Weaver (2003), Coupling of the hemispheres in observations and simulations of glacial climate change, Quaternary Science Reviews, 22(5-7), 659–671, doi:10.1016/S0277-3791(02)00184-1.

23. Schmittner, A., O. SAENKO, and A. WEAVER (2004), Response to the comments by Peter Huybers, Quaternary Science Reviews, 23(1-2), 210–212, doi:10.1016/j.quascirev.2003.08.002.

24. Siddall, M., T. F. Stocker, T. Blunier, R. Spahni, J. F. McManus, and E. Bard (2006), Using a maximum simplicity paleoclimate model to simulate millennial variability during the last four glacial periods, Quaternary Science Reviews, 25(23-24), 3185–3197, doi:10.1016/j.quascirev.2005.12.014.

25. Stocker, T. (2011), Introduction to Climate Modelling, Springer Science & Business Media.

26. Steig, E. J., and R. B. Alley (2002), Phase relationships between Antarctic and Greenland climate records, Annals of Glaciology, 35(1), 451–456, doi:10.3189/172756402781817211.

27. Stocker, T. F., and S. J. JOHNSEN (2003), A minimum thermodynamic model for the bipolar seesaw, Paleoceanography, 18(4), 1087–n/a, doi:10.1029/2003pa000920.

28. Veres, D. et al. (2013), The Antarctic ice core chronology (AICC2012): an optimized multi-parameter and multi-site dating approach for the last 120 thousand years, Clim. Past, 9(4), 1733–1748, doi:10.5194/cp-9-1733-2013.

29. Wunsch, C. (2003), Greenland—Antarctic phase relations and millennial time-scale climate fluctuations in the Greenland ice-cores, Quaternary Science Reviews, 22(15-17), 1631–1646, doi:10.1016/S0277-3791(03)00152-5.

30. Wunsch, C. (2006), Abrupt climate change: An alternative view, Quaternary Research, 65(2), 191–203, doi:10.1016/j.yqres.2005.10.006.

CHAPTER 3: POLAR CLIMATES PHASE COHERENCE THROUGH THE LAST GLACIAL PERIOD

3.1. Introduction

The polar climate proxy records from Greenland and Antarctica have been known to have a one-to-one recurring of warming events during the last glacial period [*EPICA Community Members*, 2006]. However, it is well known that the proxy records (temperature proxy, either $\delta^{18}O$ or δD) between the two poles do not share a simple lead-lag relation. Instead, a stable phase relationship centered about $\pi/2$ between them has been proposed and embedded in various conceptual models that attempt to characterize their relationship. Rial [2012] has conducted a systematic analysis of polar phase difference, demonstrating that the polar climates have been in a state of $\pi/2$ phase synchronization for the duration between 10-90 ka (kilo-years before present). The $\pi/2$ phase relation also happens to be embedded in other models that describe the relation between the polar proxy records (see [*Schmittner et al.*, 2003; *Huybers*, 2004; *Steig*, 2006], and analysis presented in Chapter 2). According to Rial [2012], a $\pi/2$ phase difference naturally accounts for the difference in the shapes of the warming events. The success in describing the polar climate relationship with simple conceptual models has led to multiple attempts to reconstruct the Greenland climate history beyond the length of the ice core record[*Siddall et al.*, 2006; *Barker et al.*, 2011].

However, reconstructing climate variations beyond the last glacial period assumes that this relationship based on the climate history of the most recent glacial period was constant beyond the previous glacial period(s), and can be applied across an interglacial. To test the validity of this assumption and, more importantly, to be able to provide a first degree estimation of the uncertainty for the reconstructed polar climate, an investigation of the robustness of the polar phase relationship is needed. Moreover, recent high resolution polar ice core proxies have revealed periods of decoupling between the Greenland climate and the low latitude hydrological variations in the sub-millennial scale, challenging the role of the Greenland record as the indicator for oceanic processes in the North Atlantic [*Guillevic et al.*, 2014; *Landais et al.*, 2015]. A detailed polar phase relationship investigation will aide in detecting periods of weak coherence, if any, thus revealing if decoupling also occurs in the millennial band of climate variation.

With the help of recent developments in unified cross-pole chronology that greatly reduced the timing uncertainty of the millennial scale events [see like *Veres et al.*, 2013], we quantify the millennial frequency band phase characteristics between the polar ice core water isotopes proxy data (namely, $\delta^{18}O$ and δD). Our results confirm the robustness of the $\pi/2$ phase relationship, which persists through majority of the last glacial period (10 – 110 ka). At the same time, we also identify instances of weak coherence, during which the phase differences between the records change abruptly and behave near randomly with a much weaker coherence. Since the strength of coherence describes the communication of climatic signals between the polar regions, the variation may involve changing circulation patterns in the intervening oceans or atmosphere. Indeed, despite the low sampling intensity towards the older section last glacial period, we demonstrate that the weak coherence tends to coincide in timing with periods of reduced/ceased ocean mixing, as revealed by the plateaus in the ε_{Nd} tracer records (defined as the $^{143}Nd/^{144}Nd$ ratio relative to a reference "bulk Earth" value) from both southeastern Atlantic and Indian Ocean [*Piotrowski et al.*, 2005; 2009]. This observation is consistent with our experiments with a coupled-relaxation oscillator, in which we determined the critical role of the ocean heat exchange in sustaining a coherent phase relation between polar records. We then further attribute the changes in the polar phase coherence to changes in the summer insolation forcing at 65°N latitude, suggesting the insolation may have been regulating the polar climate communication through the last glacial period.

We have divided our text into following parts. In the results section, we first demonstrate the close relationship between the insolation curve and the coherence curve, and then show the possible connection between the strength of the coherence to the strength of the ocean circulation. The results section is followed by the discussion, where we discussed in detail the implication of the linkage between insolation, coherence, and the ocean circulation strength. In the final methods section, we elaborate on the steps we take to obtain the mean phase coherence curve as well as the details in the conceptual model applied in this study.

3.2. Results

3.2.1. Phase coherence and its relationship with insolation forcing

The windowed mean phase coherence reveals the variation in phase coherence between polar climate records. During the last glacial period, the phase coherence has gone through stages of strong and weak coherence, with relatively smooth transitions that are likely due to the windowing process (Figure 3.1a). According to the coherence curve, the glacial period can be divided into three alternating periods of weak coherence and two long periods of strong coherence. The most recent weak coherence period spans roughly from 15 ka to 30 ka, which covers the last glacial maxima (LGM) and overlaps with the marine isotope stage 2 (MIS 2). The preceding period of 30 ka to 60 ka (coinciding with MIS 3) sees a persistent strong coherence between the polar climate records, with the most frequent recordings of abrupt climate events in the Greenland record. However, the coherence weakens greatly during the cold period of MIS 4 from 60 ka to 71ka to the level LGM. The coherence then resumes gradually during the inception of the last glacial period as some of the longest abrupt warming events took place between 71 ka to 90 ka. Prior to 90 ka, the coherence again weakens during 90-100 ka. On top of this general pattern, the coherence varies slightly within each stage. This suggests that the mechanisms of polar connection that cause this phase coherence do have natural variations. It is tempting to speculate that the high frequency variation follows the timings of the abrupt climate changes. However, such speculation could not be confirmed with current temporal resolution of our coherence curve, which is limited by the window width used when calculating the coherence.

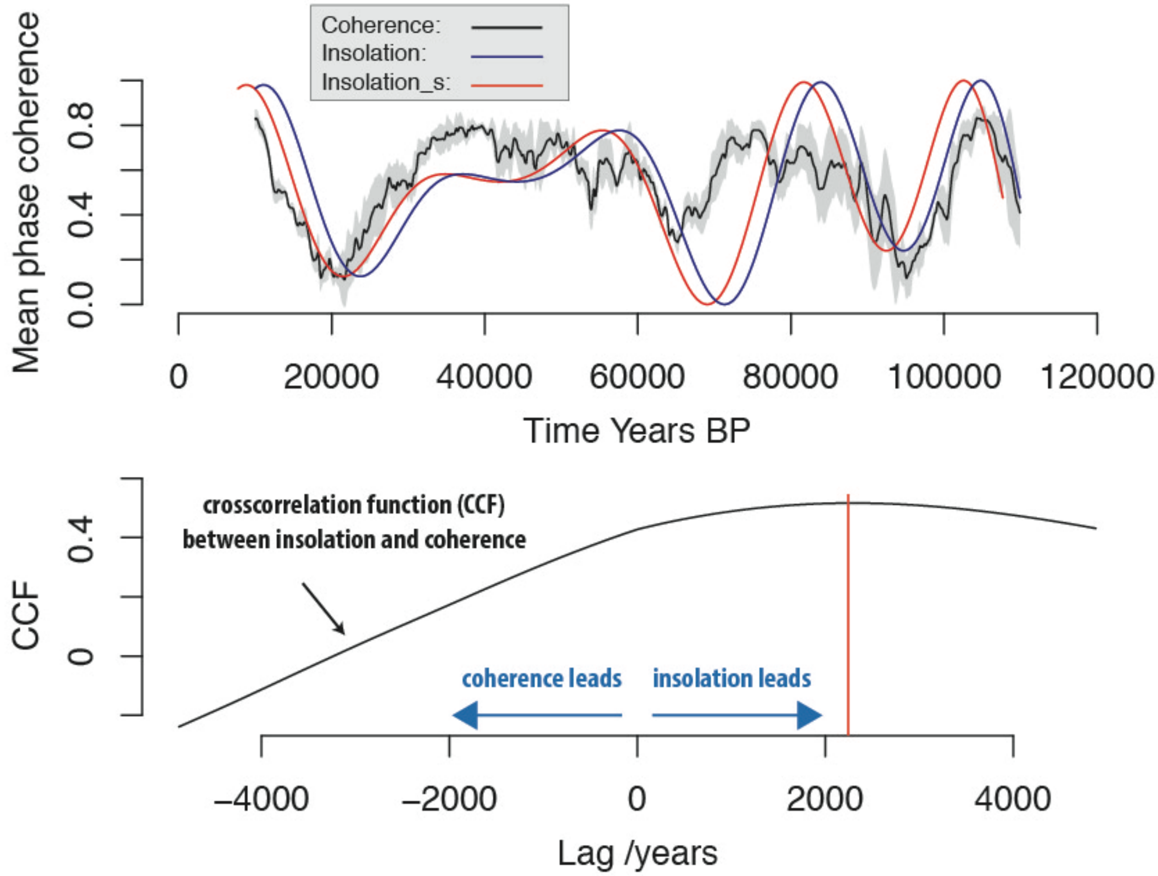

Figure 3.1. Polar phase coherence over the last glacial period. Upper panel. Black line: average phase coherence between the NGIRP $\delta^{18}O$ and the $\delta^{18}O$ or δD from four Antarctica ice cores; blue line: daily average solar radiation forcing at latitude 65°N. Scaled to compare with the coherence; red line: the same insolation forcing as the blue line but shifted by 2244 years to achieve maximum correlation between itself and the coherence curve (black line). Lower panel. Black line: cross-correlation function between the insolation and the coherence with maximum correlation at positive lag (indicated by the red line) suggesting an insolation lead over the polar coherence evolution.

Insolation forcing has long been recognized as one of the most important external forcings of the climate on the Earth. The specific summer insolation at mid-latitude (here we take the 65°N; the Matlab code we used to calculate insolation forcing is from Huybers [2006]) has been consistently used in the interpretation of climate records as it has strong influence over the growth of the mid-latitude ice sheet. We have discovered a close connection between polar climate phase coherence and the insolation variation at 65°N (Figure 3.1a). The strong connection is evidenced by observing the two curves together, where the weak coherence tends to follow the period of reduced insolation forcing (noticing the direction of time is to the left). This relationship is robust as it is able explain all three instances of weak coherence with minima in the insolation. Vice versa, strong and intermediate insolation forcing coincide with strong polar coherence that has been maintained for majority of the last glacial period. A further cross-correlation function has been applied between the insolation and the coherence curve (Figure 3.1b). The result not only confirms the presence of a lagged correlation between them, but also shows that the insolation, on average, leads the coherence by about 2000 years.

3.2.2. Phase coherence and its connection with rate of deep ocean mixing

The variation in North Atlantic Deep Water (NADW) formation and the following changes in the Atlantic Meridional Overturning Circulation (AMOC) have strong influence on the hemisphere-wide heat distribution. It has been well established that changes in AMOC strength have accompanied most of the warming events of the last glacial period [*Henry et al.*, 2016]. The AMOC runs meridionally, transferring climatic signal between the polar regions. Thus, variation in the strength of this circulation influences the strength of communication between the polar regions. In our results (Figure 3.2), we find that the low coherence periods of MIS 2 and 4 coincide with full glacial temperature in both Greenland and Antarctica records, during which periods millennial scale warming events are found lacking. Concomitantly, these periods also see a reduction in the mixing of water masses between North Atlantic Deep Water (NADW) and Antarctic Bottom Water (AABW) in ε_{Nd} records from both the southeastern Atlantic (RC11-83/TN057-21) [*Piotrowski et al.*, 2005; 2008] and the Indian Ocean (Core SK129) [*Piotrowski et al.*, 2009; *Wilson et al.*, 2015]. In contrast, strong coherence tends to occur during relatively warm periods of the glacial climate, during which, frequent abrupt warming events took place. Accordingly, during periods of strong coherence, the deep ocean water mixing strengthened, indicated by the frequent variations (increase in variance) in the corresponding ε_{Nd} records. The period of weak coherence between 90 to 100 ka may follow the same pattern, however, due to the low sampling rate at this old section of the ε_{Nd} record, it is not possible to make any firm conclusion.

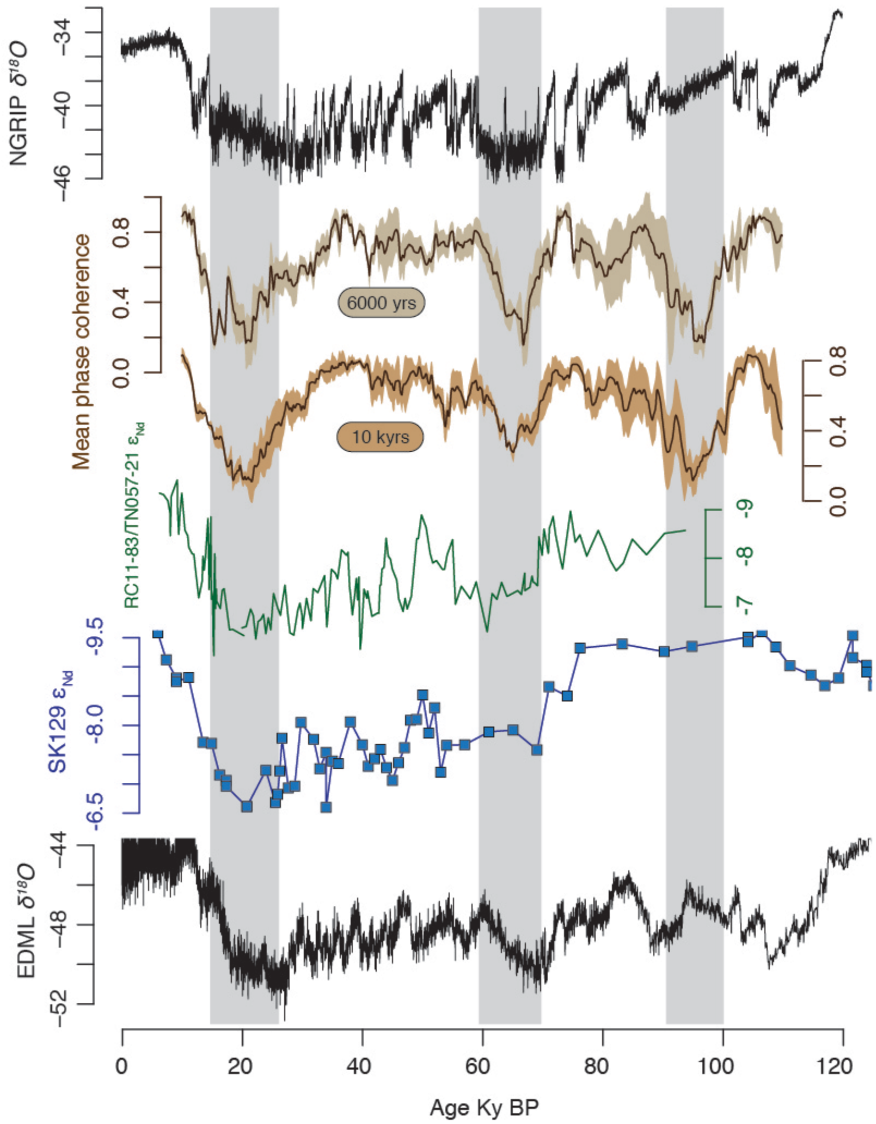

Figure 3.2. Polar phase coherence and the rate of ocean mixing. From top to bottom. 1) NGRIP $\delta^{18}O$ record [*Veres et al.*, 2013]; 2) Mean phase coherence between NGRIP and for Antarctica ice core records (EDML, EDC, VOSTOK, TALDICE) calculated with a moving window of width 6000 years; 3) The same to 2) but with window width 10 thousand years; 4) ε_{Nd} composite record from southeastern Atlantic sediment core RC11-83/TN057-21 [*Piotrowski et al.*, 2005]; 5) ε_{Nd} record from Indian Ocean sediment core SK129 [*Wilson et al.*, 2015]; 6) EDML $\delta^{18}O$ record [*Veres et al.*, 2013]. Vertical grey bars show periods of weak polar phase coherence. All the ice cores (that is including the NGRIP and the four Antarctica records) and the coherence curves derived from them are on the AICC2012 chronology. The others are on their own respective chronologies (please refer to their original publications).

3.2.3. The oceanic control of the simulated polar climate phase coherence

Finally, to test our hypothesis that the ocean circulation strength is able to influence the polar phase coherence, we have utilized a conceptual model built upon the coupling of two nonlinear relaxation oscillators. Each oscillator is a Van der Pol oscillator and is able to reproduce both the characteristic saw-tooth shape of the Greenland isotope record and the triangular Antarctic record [*Rial*, 2012; *Oh et al.*, 2014]. The same type of model has been frequently used in paleoclimate research to simulate the 100,000 year late Pleistocene glaciation [*Saltzman et al.*, 1981] and the $\pi/2$ phase relation between polar records [*Rial*, 2012]. The two coupled oscillators are assigned their roles as representing the north (Greenland, oscillator 1) and the south (the Antarctica, oscillator 2), respectively. In each oscillator, the variations in the sea ice extent (idealized as the latitude of the sea ice margin towards equator) and the mean ocean temperature are calculated. The two oscillators are coupled through the difference in both mean ocean temperature (reactive coupling) and rate of mean ocean temperature change (dissipative coupling) with parameters q_1 and q_2 controlling the strength of dissipative coupling and reactive coupling, respectively.

To investigate the effect of coupling strength on the final phase coherence between the simulated polar records, each coupling parameter has been isolated (by assuming the other coupling strength zero) and incrementally increased. For each coupling strength, the cVDP model has been run for 100 kilo-year (ky) five times, each with a random set of initial conditions for $\{u_1, u_2, u_3, u_4\}$ (see model details in the following Methods section). The length of the simulation was set to 100 ky to reduce influence from the initial transient period.

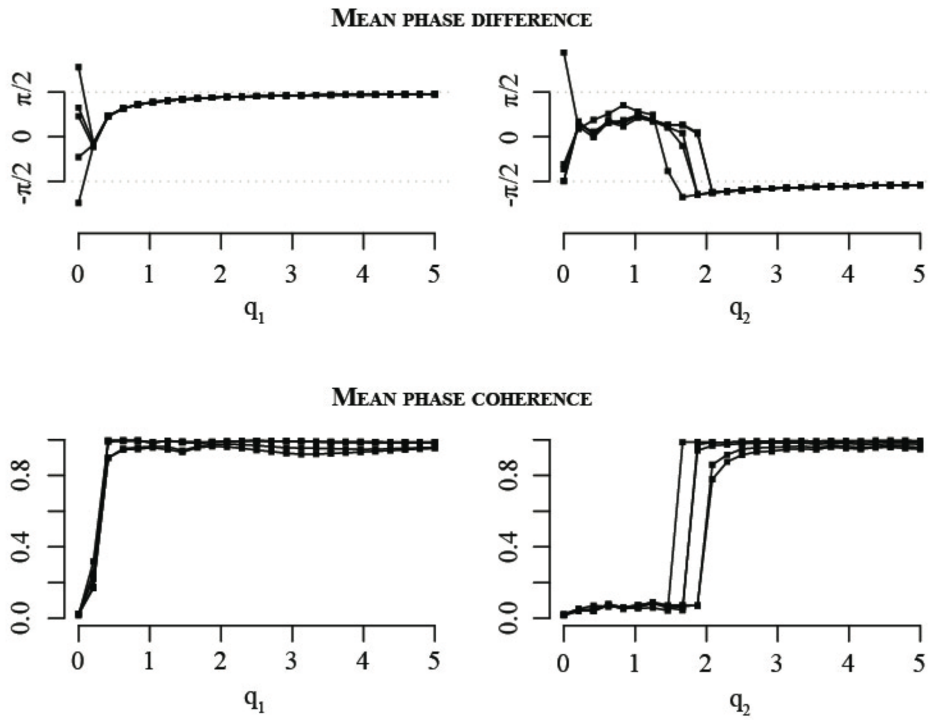

Figure 3.3. The influence from the coupling parameters on the phase synchronization between the two oscillators. The natural frequencies of oscillator 1 and 2 are 1/1500 $year^{-1}$ and 1/3000 $year^{-1}$. When testing q_1, the value of q_2 was kept 0. The same is true when testing q_2. For each q value, five sets of random initial conditions are set to start the simulations, and the phase difference and phase coherence were calculated.

From the testing results (Figure 3.3), we conclude that, given sufficiently large coupling strength, both coupling parameters q_1 and q_2 can independently achieve phase synchronization between the two oscillators. It is also important to notice that, even with different assigned natural frequencies between oscillator 1 ($1/1500$ year^{-1}) and oscillator 2 ($1/3000$ year^{-1}), synchronization can be achieved with sufficiently strong coupling through increasing either q_1 or q_2. However, when synchronization is obtained, q_1 and q_2 result in different phase difference. With increasing q_1, the phase difference between oscillator 1 and oscillator 2 stabilizes at $\pi/2$. On the contrary. Increasing q_2 lead to a $-\pi/2$ phase difference. From the polar records, we learnt that the phase difference is centered around $\pi/2$. If we assume the model gives a reasonably good representation of the large-scale interactions between the polar climates through the intervening ocean, then the consistencies between the phase relationships of the ice core records and the simulations controlled by q_1 could suggest that the difference in the rate of change in the mean ocean temperature (dissipative coupling) between respective oceans plays a greater role. To put this in terms of the actual physical system, the model results show that it is not the difference in absolute ocean temperature, but rather the asymmetric heat (rate of change of temperature) distribution/transfer between the north and south which plays a key role in regulating polar climate connection.

3.3. Discussion

In this study, we have estimated the history of the phase coherence between the polar climate records for last glacial period. Our results show that the coherence between the polar climates, despite being centered at $\pi/2$ for majority of the time with strong coherence, has undergone difference stages of strong and weak lock. Moreover, our analysis revealed an important connection between solar insolation input, the polar climate coherence, and the circulation strength of the ocean. Specifically, we have demonstrated a lagged correlation between the insolation and the polar climate phase coherence, suggesting an insolation control over the communication between the polar climates. We also showed that variation in phase coherence is in general consistent with the strength of the ocean circulation changes indicated by ε_{Nd} records from both southeastern Atlantic and Indian Ocean. With the help of a coupled Van der Pol oscillators, we propose that the variation in phase coherence is likely due to the changing magnitude of heat exchange in the intervening oceans between the poles. With strong heat exchange corresponding to strong coherence with $\pi/2$ phase synchronization between the polar climates, where there is a weak or stagnant ocean mixing, reducing heat exchange, it leads to a weak coherence.

The climate of the Greenland has been known for its tight connection with the sedimentary records extracted in the North Atlantic region [*Shackleton et al.*, 2000]. And the Greenland ice core records have long been used to estimate the state of oceanic process (like deep water formation), as well being used as template for wiggle matching many of the climate signals from North Atlantic region that contain potential D/O-like signal. However, recent discoveries based on high resolution records challenge the role of the Greenland record as the indication for oceanic process or hydrological processes in the low latitude [*Guillevic et al.*, 2014; *Landais et al.*, 2015]. It has been shown that Greenland's climate has been decoupled from the hydrological processes in the tropical region multiple times during the last glacial period [*Guillevic et al.*, 2014]. We do not expect to see this type of decoupling in our coherence result because it appears in the centennial scale. Nonetheless, our results demonstrated that weak coherence between Greenland and Antarctica took place in the millennial band, indicating periods that Greenland climate had a rather regional influence. Periods of reduced deep ocean mixing reflected in the ε_{Nd} record indicate less interaction between the two poles, thus the weaker coherence. This observation is consistent with our model analysis, in which with weaker coupling, strong coherence cannot be sustained.

Unlike the well-known connection between the polar climate (especially Greenland's climate) and ocean circulation, Milankovitch frequency has long been proven to be an important factor in regulating the glacial-interglacial climate variation, though its connection with millennial scale polar climate changes has remained unknown. Even the shortest periodicity of the Milankovitch insolation variation is of the scale of 20 thousand years, which is at very different scale to directly influence the climatic events happens at millennial scale. Rial and Saha [2011] successfully simulated Greenland's NGRIP $\delta^{18}O$ record by forcing a stochastic Van der Pol oscillator with 65°N summer insolation forcing. It successfully demonstrated that nonlinear processes like amplitude or frequency modulation can influence events across scales, thus bridging the high frequency millennial climate change with the orbital scale insolation change. Our results showed that the insolation may have an even broader influence on the polar climate, in which it regulates the millennial scale polar climate phase coherence. The proposed polar climate phase synchronization has been sustained for most of the glacial period with strong coherence, except for the periods with minimum insolation forcing. And unlike the frequency/amplitude modulation required to simulate the Greenland record, the insolation and coherence seems to maintain a simple linear relationship with a fixed lag. Although the exact pathway the insolation followed to regulate the communication of the polar climate remains unknown, such a pathway is very likely to involve the dynamics of the northern mid-latitude ice sheets, as they are very sensitive to the summer insolation change at 65°N. But it is unclear whether the insolation is able to directly influence the oceanic processes to affect the inter-polar communication of climatic signal.

3.4. Conclusion

Our study presents the first detailed look at the evolution of the phase coherence between polar climates. With dominant, strong, phase coherence centered at $\pi/2$, we discovered times of weak coherence during which the polar climates may have had insufficient communication (weak coupling strength in the model, and reduced ocean mixing rate) to sustain a strong coherent phase relation. During these times, Greenland may have had reduced communication beyond its regional influence, thus the climate records from Greenland may not be appropriate to be used as template for wiggle-matching of the Atlantic records. Further analysis reveals a strong insolation control over the polar climate coherence, suggesting the potential cause of change in inter-polar climate signal transfer, thus the change in oceanic circulation from the variations in solar insolation forcing.

Based on the results and analysis presented above, we strongly recommend caution when trying to reconstruct polar climate history from each other assuming a single form of relationship. The strong linkage between insolation and polar climate phase coherence can be used to gauge the uncertainty when reconstructing polar climate from each other, with times of insolation minima likely corresponds to greater uncertainty in the millennial scale reconstruction. The penultimate glacial periods have been shown to have less millennial scale climate variations [*Obrochta et al.*, 2014]. So if the observation we have made based on last glacial period can be extended to this period, the millennial scale reconstruction for this period could have greater uncertainty than previously expected.

3.5. Method

3.5.1. Isolate millennial scale variations through filtering

The paleoclimate records are well known for their presence of broad band frequency content. However, the concept of both instantaneous frequency/phase or and the mean phase coherence are built upon the property of narrow band signal. In order to isolate the millennial scale variations, we have applied a 4^{th} order butterworth bandpass filter with corner frequency [1/10000, 1/1000] $year^{-1}$ to each of the ice core records. By filtering the signal to the millennial scale, the direct influence from the long period Milankovitch forcing and that from the high frequency weather signal should be greatly reduced.

3.5.2. Mean phase coherence

Mean phase coherence is a statistic measure based on the difference in instantaneous phases between signals [*Mormann et al.*, 2000]. It has advantages over the direct instantaneous phase difference in providing only the phase difference, but also the strength of the coherence. With the instantaneous phase differences between two signals being coherent, meaning that majority of them being the close to a certain fixed value, the addition of their complex phase representation will be constructive and its coherence value close to 1. On the other hand, if the phase differences are divergent, their mean phase coherence will be close to 0 due to the lack of a unified phase angle. However, mean phase coherence does not provide temporal evolution of the phase difference. This can be circumvented by implementing the mean phase coherence with a moving window. This way, the evolution of the phase coherence can be extracted with certain compromise in the temporal resolution.

3.5.3. Coupled VDP

The Van der Pol oscillator, as one of the most representative relaxation oscillators, has been used wide in modeling climatic behavior of various scales [*Saltzman et al.*, 1981; *Rial and Saha*, 2011; *Rial*, 2012; *Daruka and Ditlevsen*, 2015]. Saltzman et al. [1981] have derived the simplified climate oscillation to a Van der Pol oscillator, with two variables representing the latitudinal polar ice extend and the mean ocean temperature, and through which they have simulated the 100 ky late Pleistocene glacial cycle. More recently, Rial [2012] further developed Saltzman's Van der Pol model, and extended it by coupling two such oscillators through both reactive and dissipative terms between the mean ocean temperature variables (refer to as Rial12 in the following discussion). Each of the oscillators in Rial12 is representing one polar region. By coupling through the difference in the ocean temperature and the difference in rate of change of the ocean mean temperature terms, the Rial12 was used to simulate the characteristics of climate records from both poles. Rial [2012] has observed that the simulated polar climate oscillations share the same phase synchronization relationship as that seen from the ice core records. Here, we have tested the effective coupling that gives rise to the synchronization state via varying increase the coupling parameters q_1 and q_2 from 0 (uncoupled) to certain positive values that sustain stable phase relationship between the simulated polar records.

$$u_1'(t) = -\omega_1^2 u_2(t) + M_1(t) + \zeta(t)$$

$$u_2'(t) = f_1(t, u_1, u_2) + p(q_1, q_2, u_1', u_3', u_1, u_3)$$

$$u_3'(t) = -\omega_2^2 u_4(t) + M_2(t) + \eta(t)$$

$$u_4'(t) = f_2(t, u_3, u_4) - p(q_1, q_2, u_1', u_3', u_1, u_3)$$

$$p(q_1, q_2, u_1{}', u_3{}', u_1, u_3) = q_1[u_1{}'(t) - u_3{}'(t)] + q_2[u_1(t) - u_3(t)]$$

$$f_1(t, u_1, u_2) = \mu_1[u_2(t) - \frac{1}{3}u_2^3(t)] + u_1(t)$$

$$f_2(t, u_3, u_4) = \mu_2[u_4(t) - \frac{1}{3}u_4^3(t)] + u_3(t)$$

where

- ω_1 and ω_2 are the natural radian frequencies of the oscillator 1 and 2 respectively;
- $M_1(t)$ and $M_2(t)$ are the external forcing to the oscillator 1 and 2, they were set to zero in our analysis;
- $\zeta(t)$ and $\eta(t)$ are white noise as stochastic term, they were also set to zero for simplicity;
- μ_1 and μ_2 control the nonlinearity of the oscillator 1 and 2 respectively;
- q_1 and q_2 are coupling strength between the oscillator 1 and 2.

REFERENCES

1. Barker, S., G. Knorr, R. L. Edwards, F. Parrenin, A. E. Putnam, L. C. Skinner, E. W. Wolff, and M. Ziegler (2011), 800,000 years of abrupt climate variability, *Science*, *334*(6054), 347–351, doi:10.1126/science.1203580.

2. Daruka, I., and P. D. Ditlevsen (2015), A conceptual model for glacial cycles and the middle Pleistocene transition, *Climate dynamics*, *46*(1-2), 29–40, doi:10.1007/s00382-015-2564-7.

3. EPICA Community Members (2006), One-to-one coupling of glacial climate variability in Greenland and Antarctica, *Nature*, *444*(7116), 195–198, doi:10.1038/nature05301.

4. Guillevic, M. et al. (2014), Evidence for a three-phase sequence during Heinrich Stadial 4 using a multiproxy approach based on Greenland ice core records, *Climate of the Past*, *10*(6), 2115–2133, doi:10.5194/cp-10-2115-2014.

5. Henry, L. G., J. F. McManus, W. B. Curry, N. L. Roberts, A. M. Piotrowski, and L. D. Keigwin (2016), North Atlantic ocean circulation and abrupt climate change during the last glaciation, *Science*, *353*(6298), 470–474, doi:10.1126/science.aaf5529.

6. Huybers, P. (2004), Comments on "Coupling of the hemispheres in observations and simulations of glacial climate change" by A. Schmittner, O.A. Saenko, and A.J. Weaver, *Quaternary Science Reviews*, *23*(1-2), 207–210, doi:10.1016/j.quascirev.2003.08.001.

7. Huybers, P. (2006), Early Pleistocene glacial cycles and the integrated summer insolation forcing, *Science*, *313*(5786), 508–511, doi:10.1126/science.1125249.

8. Landais, A. et al. (2015), A review of the bipolar see–saw from synchronized and high resolution ice core water stable isotope records from Greenland and East Antarctica, *Quaternary Science Reviews*, *114*, 18–32, doi:10.1016/j.quascirev.2015.01.031.

9. Mormann, F., K. Lehnertz, P. David, and C. E. Elger (2000), Mean phase coherence as a measure for phase synchronization and its application to the EEG of epilepsy patients, *Physica D*, *144*(3-4), 358–369.

10. Obrochta, S. P., T. J. Crowley, J. E. T. Channell, D. A. Hodell, P. A. Baker, A. Seki, and Y. Yokoyama (2014), Climate variability and ice-sheet dynamics during the last three glaciations, *Earth and Planetary Science Letters*, *406*, 198–212, doi:10.1016/j.epsl.2014.09.004.

11. Oh, J., E. Reischmann, and J. A. Rial (2014), Polar synchronization and the synchronized climatic history of Greenland and Antarctica, *Quaternary Science Reviews*, *83*, 129–142, doi:10.1016/j.quascirev.2013.10.025.

12. Piotrowski, A. M., S. L. Goldstein, S. R. Hemming, and R. G. Fairbanks (2005), Temporal relationships of carbon cycling and ocean circulation at glacial boundaries, *Science*,

307(5717), 1933–1938, doi:10.1126/science.1104883.

13. Piotrowski, A. M., S. L. Goldstein, S. R. Hemming, R. G. Fairbanks, and D. R. Zylberberg (2008), Oscillating glacial northern and southern deep water formation from combined neodymium and carbon isotopes, *Earth and Planetary Science Letters*, *272*(1-2), 394–405, doi:10.1016/j.epsl.2008.05.011.

14. Piotrowski, A. M., V. K. Banakar, A. E. Scrivner, H. Elderfield, A. Galy, and A. Dennis (2009), Indian Ocean circulation and productivity during the last glacial cycle, *Earth and Planetary Science Letters*, *285*(1-2), 179–189, doi:10.1016/j.epsl.2009.06.007.

15. Rial, J. A. (2012), Synchronization of polar climate variability over the last ice age: in search of simple rules at the heart of climate's complexity, *Am J Sci*, *312*(4), 417–448, doi:10.2475/04.2012.02.

16. Rial, J. A., and R. Saha (2011), *Modeling Abrupt Climate Change as the Interaction Between Sea Ice Extent and Mean Ocean Temperature Under Orbital Insolation Forcing*, Geophysical Monograph Series, American Geophysical Union, Washington, D. C.

17. Saltzman, B., A. Sutera, and A. Evenson (1981), Structural Stochastic Stability of a Simple Auto-Oscillatory Climatic Feedback System, *J. Atmos. Sci.*, *38*(3), 494–503, doi:10.1175/1520-0469(1981)038<0494:SSSOAS>2.0.CO;2.

18. Schmittner, A., O. A. Saenko, and A. J. Weaver (2003), Coupling of the hemispheres in observations and simulations of glacial climate change, *Quaternary Science Reviews*, *22*(5-7), 659–671, doi:10.1016/S0277-3791(02)00184-1.

19. Shackleton, N. J., M. A. Hall, and E. Vincent (2000), Phase relationships between millennial-scale events 64,000–24,000 years ago, *Paleoceanography*, *15*(6), 565–569, doi:10.1029/2000PA000513.

20. Siddall, M., T. F. Stocker, T. Blunier, R. Spahni, J. F. McManus, and E. Bard (2006), Using a maximum simplicity paleoclimate model to simulate millennial variability during the last four glacial periods, *Quaternary Science Reviews*, *25*(23-24), 3185–3197, doi:10.1016/j.quascirev.2005.12.014.

21. Steig, E. J. (2006), Climate change: The south-north connection, *Nature*, *444*(7116), 152–153, doi:10.1038/444152a.

22. Veres, D. et al. (2013), The Antarctic ice core chronology (AICC2012): an optimized multi-parameter and multi-site dating approach for the last 120 thousand years, *Clim. Past*, *9*(4), 1733–1748, doi:10.5194/cp-9-1733-2013.

23. Wilson, D. J., A. M. Piotrowski, A. Galy, and V. K. Banakar (2015), Interhemispheric controls on deep ocean circulation and carbon chemistry during the last two glacial cycles, *Paleoceanography*, *30*(6), 621–641, doi:10.1002/2014PA002707.

APPENDIX 1

Synchronization of polar climates

Synchronization is a common phenomenon in engineering and science that emerges, for instance, when two, nonlinear, coupled oscillators progressively adapt their (originally different) natural frequency to each other until they begin to oscillate at the same frequency with constant phase difference. While commonly studied in other disciplines, the role of synchronization in climate behavior is only beginning to be explored. One area that has begun to be explored is the important evidence that the climatic interaction between the poles can be defined by a $\pi/2$ (90°) phase shift, with which the Antarctic leads the Greenland records (Figure S1). An accurate value of the shift has been obtained fitting timescales with matched methane records from both poles [*EPICA Community Members*, 2006; *Steig*, 2006].

Recent studies [*Rial*, 2012; *Oh et al.*, 2014] confirm the $\pi/2$ shift and suggest that many of the known polar climate relationships, including the bipolar seesaw, can be explained if, during the last ice age and likely in earlier times, millennial scale temperature changes of the north and south Polar Regions coupled through mutual ocean and atmospheric influences and became synchronized (frequency and phase entrained), creating a global, internal oscillation of the ocean-atmosphere-cryosphere system.

One simple way to transform a northern record into a southern one is by time integrating the northern record [*Oh et al.*, 2014], which closely reproduces the southern time series. The opposite transformation, the time derivative of the southern record, is unfortunately too noisy to be useful. One could argue that the abrupt northern warming events are proportional to the time rate of change (the time derivative) of southern temperature, a plausible argument for cause-effect relationship between polar climates. However, a more likely alternative is polar synchronization. This is because, though time integration from present to past induces the observed $\pi/2$ phase lead of Antarctica, the amplitudes obtained by time integrating the Greenland record (or differentiating the Antarctic record) are too large (or too small) as compared to the observed. In contrast, the phase shift introduced by synchronization preserves the amplitude levels of both records, consistent with the observed temperature ranges, which are very similar in both poles.

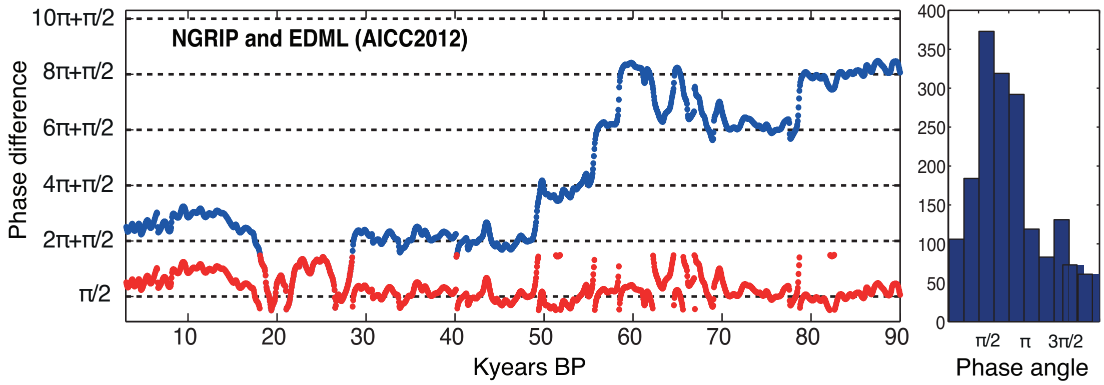

Figure S1.1. Phase difference between NGRIP (Greenland) and Antarctica's EDML isotope records calculated using the AICC2012 age model [*Veres et al.*, 2013] (blue dots). The evolution of the phase difference with the 2π jumps removed is shown in the lower part of the plot (red dots). The persistence of the $\pi/2$ phase shift is a condition for the signals to be considered synchronized. Histograms show that the distribution of phase differences strongly peaks at $\pi/2$ (mod 2π). Similar phase difference relation have been observed between methane age-matched NGRIP and DOME C, and between GRIP and BYRD (see Figure 3 in [*Oh et al.*, 2014]). It should also be noticed that the phase difference exists for all values from 0 to 2π in the histogram and synchronization in nature is rarely if ever perfect. The jumps in the phase difference (blue dots) are usually known as phase slippage.

Monte Carlo age model matching

We have used age-matching method and data from Oh et al. [2014] to unify different age models that have been attached to ice cores used in this paper. In Oh et al. [2014], a Monte Carlo scheme has been developed to match age model of an ice core to that of a methane matched ice core published by Blunier and Brook [2001]. In [*Blunier and Brook*, 2001], two ice cores from the Greenland (GRIP and GISP2) and one ice core from the Antarctica (BYRD) have been matched through the fast-varying methane gas. Isotope records from four extra ice cores (NGRIP matched to GRIP; VOSTOK, FUJI, and DOME C matched to BYRD) have been matched to this relative age model by matching to the methane matched ones by Oh et al. [2014]. For each matching between a candidate record A and a reference record B (B is methane matched and serves as a reference record), the following steps have been taken:

1. Interpolate both A and B to a common 50-year sampling interval;
2. Generate N-1 random number ranging from -49 to 49 (N is the length of the records after interpolation), which is chosen so that points will keep their original order;
3. Adjust the interval size by adding the random number series to the 50-year intervals of record A;
4. Calculate the new age model for A based on the new intervals, resulting in A^*;
5. Interpolate A^* to the same 50-year sampling interval as B;
6. Save the correlation between A^* and B;
7. Repeat steps 2-6 100000 times and pick the A^* having the highest correlation with B.

As showing in Figure S1.2, our method of age-matching significantly decreased the timing variation for records from the same polar region. The resulting age matched records have proved to be critical to the results in this paper, as the S-N temperature difference results using records' original age models has been compared to that from age-matched records in Figure S1.3.

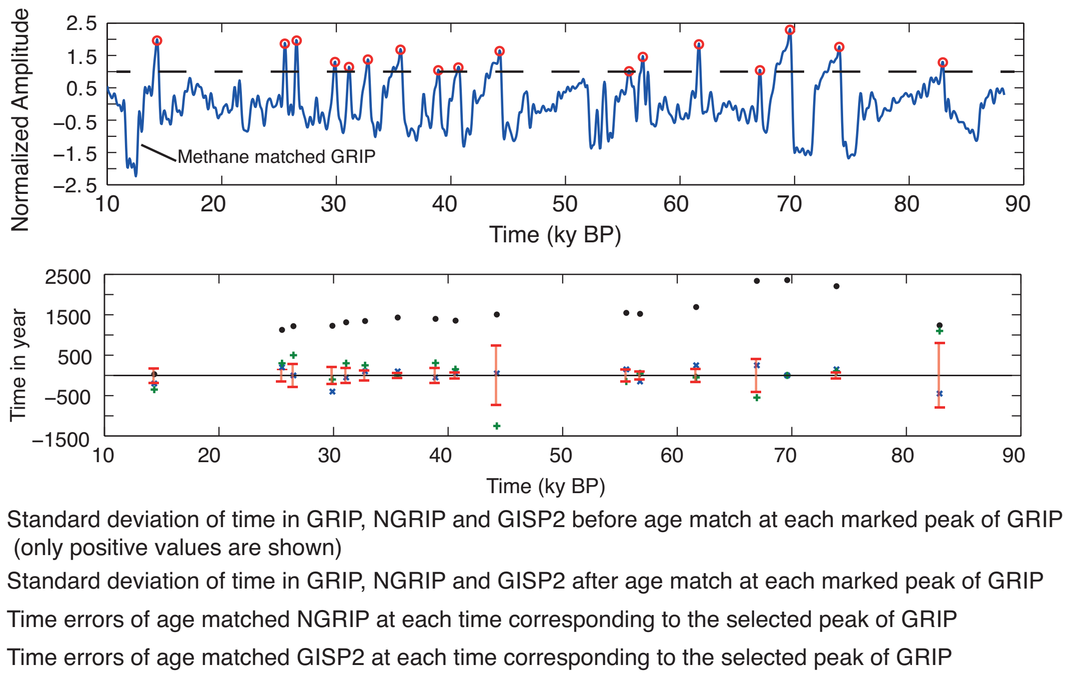

Figure S1.2. Comparison of time errors after age-match to the time errors without age-match. For the timing comparison, 17 peaks that have amplitudes greater than one standard deviation (marked with red circles in the bottom figure) were selected from methane matched GRIP records. Age matching results reduce time errors (standard deviations) from ±2400 years to less than ±400 years at the corresponding peak amplitudes, except 2 peak points that possibly due to the low sampling rate of GISP2 at these locations.

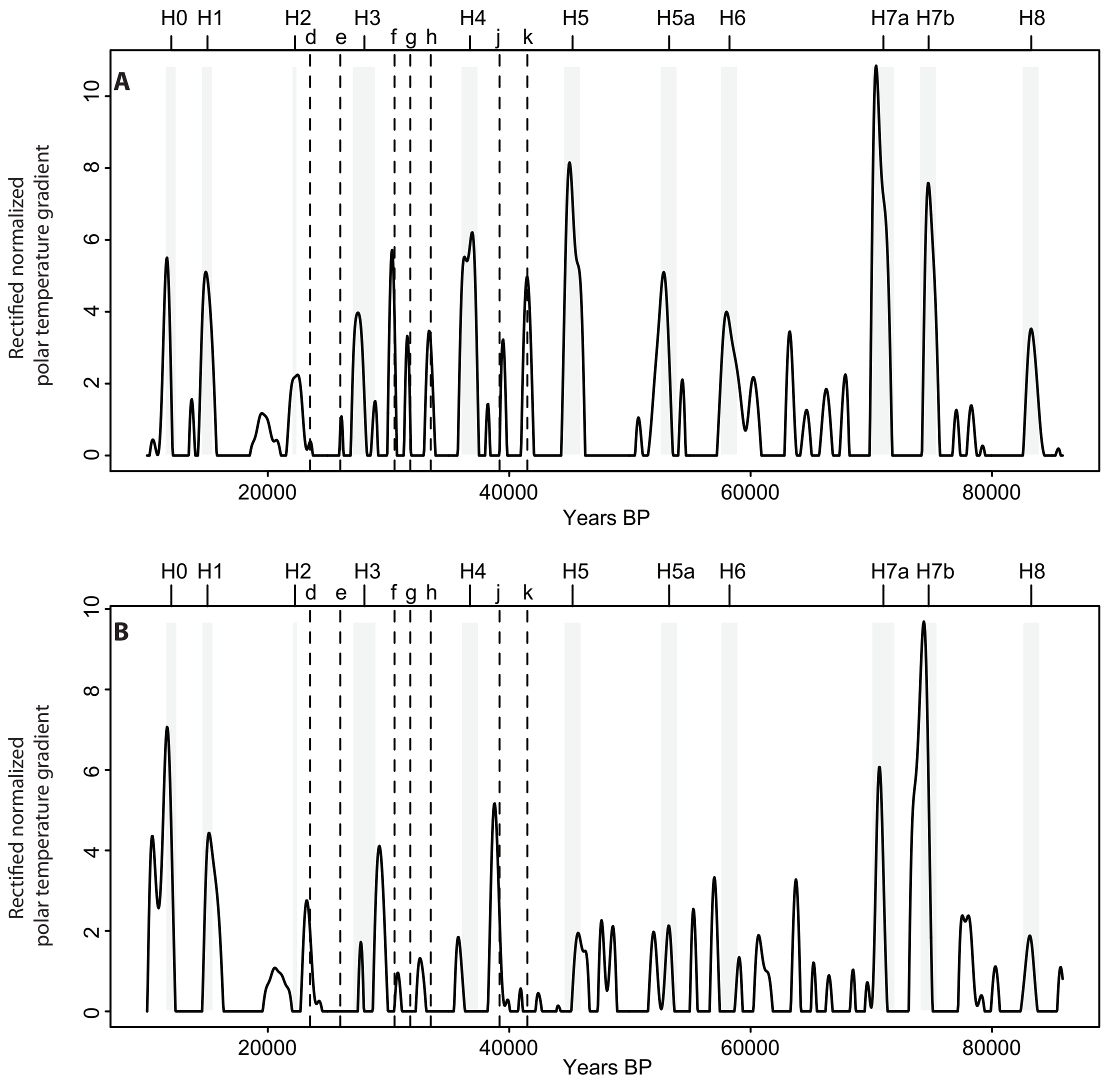

Figure S1.3. Polar climate difference calculation based on age-matched records (a) and unmatched original records (b). The peaks in the matched records align much better with occurrence of H events and IRDs when compared with the same calculation based on unmatched records, demonstrating the importance of a unifying age model when comparing polar climate history. Lower panel (b) demonstrates that the delicate $\pi/2$ polar synchronization relationship, thus the predictive power of the polar temperature gradient calculation, demolishes if the original age model of the two records were used. Two records used here are NGRIP and DOME C.

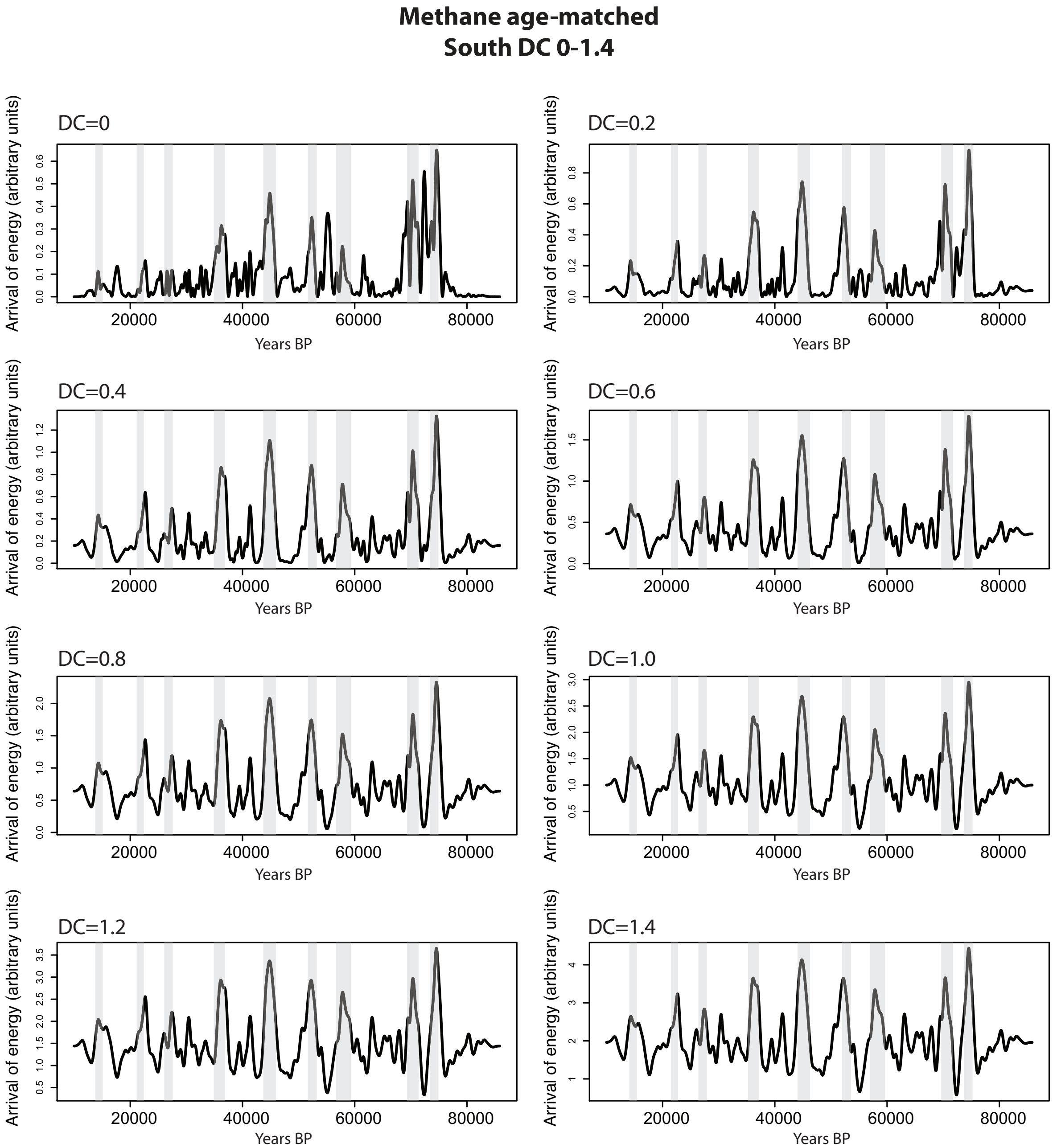

Figure S1.4. Variations in the baseline of the southern records and their impact on the power estimation. A sequence of shift values (0, 0.2, 0.4, 0.6, 0.8, 1.0, 1.2, 1.4) have been added to the averaged southern records; each of the resulting shifted record then was used to calculate power estimation. One can observe that, with a slight boost in the baseline value (≥ 0.2), the resulting power estimation became much more clean, at the same time, has a much stronger correlation with the timings of H events.

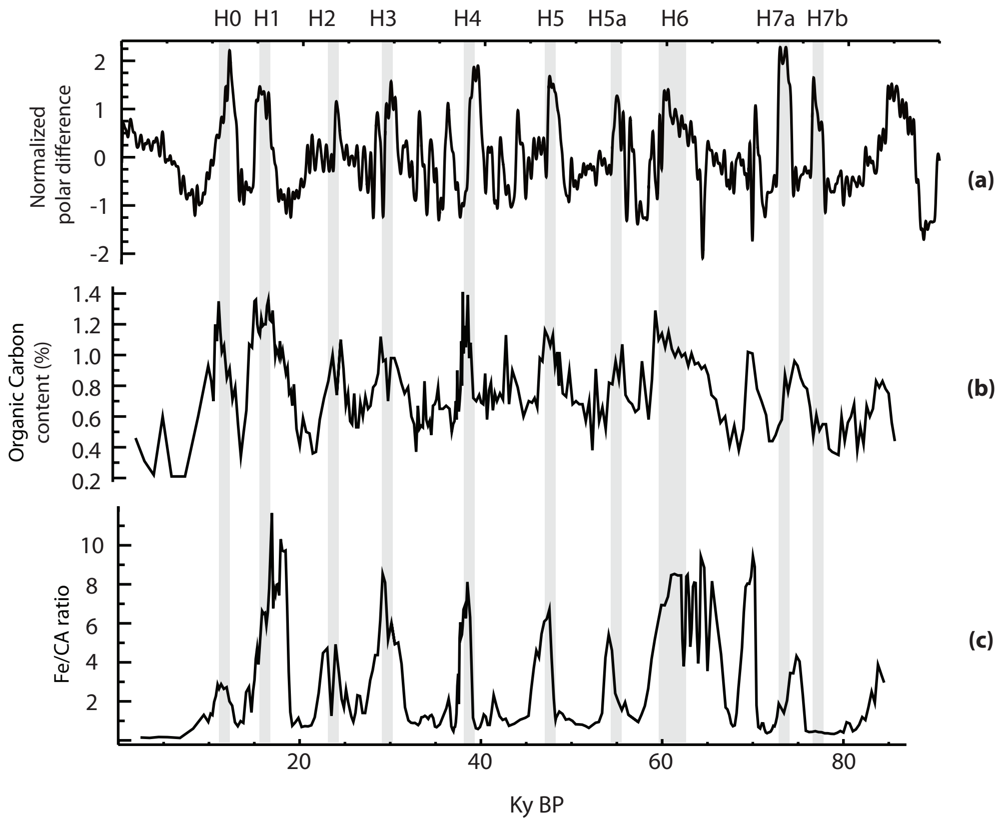

Figure S1.5. Comparison between S-N polar temperature gradient and two proxy records (organic carbon and Fe/Ca ratio) from GeoB3912-1b [*Jennerjahn et al.*, 2004] sediment core in equatorial Atlantic. After removing the high frequency variations in (a) and (b), the correlation coefficient can reach as great as 0.8. Despite the possible error introduced by different age models, such similarity suggests transmission of polar climate signal across the equator.

Analytic signal

An analytic signal (AS) is a mathematical construct that generates a complex signal out of a real one. The real part of the AS is the original signal and its imaginary part is its Hilbert transform. The components of this complex signal, surprisingly, seem to appear naturally in the polar records. In fact, we can define an analytic signal $s(t)$ associated to the Antarctic record $a(t)$, is given by $s(t) = a(t) + iH[a(t)] \approx a + ig(t)$ ($g(t)$denotes the Greenland record). Similarly, the AS associated to $g(t)$ can be written $w(t) = g(t) - ia(t)$. In other words, since $s(t) = iw(t)$ the time series of the ice core proxy records from the Polar Regions can be thought of as the real and imaginary parts of an analytic signal, or, approximately, as signals in quadrature. The real and imaginary parts of $s(t)$ have identical spectra and autocorrelation, which is nearly true in the actual proxy time series. An AS is a complex function from which the envelope, phase and energy of the original time series can be obtained [*Heyser*, 1971]. Of course, these properties are only approximately true in the real data, yet in this particular case, nature appears to closely follow mathematics, which suggests that a simple calculation of the total power of the signal can be obtained as shown in the text. Squaring amplitudes results in amplitude errors approximately double the original (in percent, for small error), but most original measurement errors are not reported or deemed too small to be discerned in time series plots. Errors in the timings of the energy calculation are not affected by the squaring of amplitudes and should be the same as the original age-matched data.

APPENDIX 2

Model details

Integration/Differentiation model (I/D)

The conceptual model used in [Schmittner et al. 2003] is the following

$$\frac{\partial A(t)}{\partial t} = -sG(t)$$

converting it to discrete form

$$A(i) = \sum_{k=0}^{i} G\,(k) * dt$$

$$G(i) = (A(i) - A(i-1))/dt$$

Thermal Bipolar Seesaw model (TBS)

The model presented in [Stocker and Johnsen, 2003]

$$A(t) = -\frac{1}{\tau}\int_0^t G(t-t')\exp(-t'/\tau)dt' + A(0)\exp(-t/\tau)$$

converting to its discrete form

$$A(i) = -\frac{1}{\tau}\sum_{k=0}^{i} G\,(i-k)\exp(-k/\tau) + A(0)\exp(-i/\tau)$$

$$G(i) = -A(i) - \tau\frac{A(i-1) - A(i)}{dt}$$

Phase Synchronization model (PhaseSync)

$$A(i) = G(i) \otimes h_{G\to A}(i)$$

$$G(i) = A(i) \otimes h_{A\to G}(i)$$

For even number of points:

$$h_{G\to A}(i) = \frac{2}{N}\sin(\frac{i}{2}\pi)^2\cot(\frac{i}{N}\pi)$$

For odd number of points:

$$\boldsymbol{h_{G\to A}(i) = \frac{1}{N}[\cot(\frac{i}{N}\pi) - \frac{\cos i\pi}{\sin(\frac{i}{N}\pi)}]}$$

In these equations,

- $A(t)$: the Antarctica climate signal. $A(i)$ is its discrete form.
- $G(t)$: the Greenland climate signal. $G(i)$ is its discrete form.
- $-G(i)$: the climate signal in the South Atlantic according to bipolar seesaw model.
- τ: the characteristic timescale.
- $\otimes$: convolution symbol.

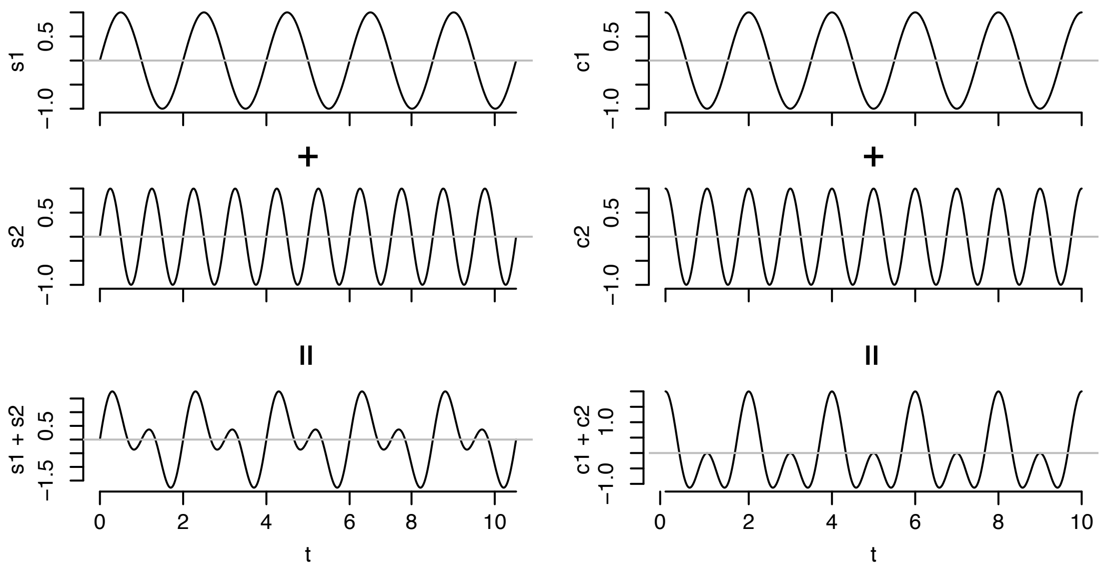

Figure S2.1. Illustration of the phase shift concept. s1 and c1 are sine and cosine function both with frequency 0.5, but with a phase difference of $\pi/2$ between them; the same is true with s2 and c2, which have double the frequency (f = 1) compared to the s1 and c1 pair. While a simple time shift of one quarter of their corresponding period can transform s1 to c1 or s2 to c2, their respective sums (s1 + s2) and (c1 + c2), still have a phase shift of $\pi/2$, cannot be transform into each other by simple shift in time. As in the case of the polar climate records, the sums from sine and cosine function have very distinct shape characteristics.

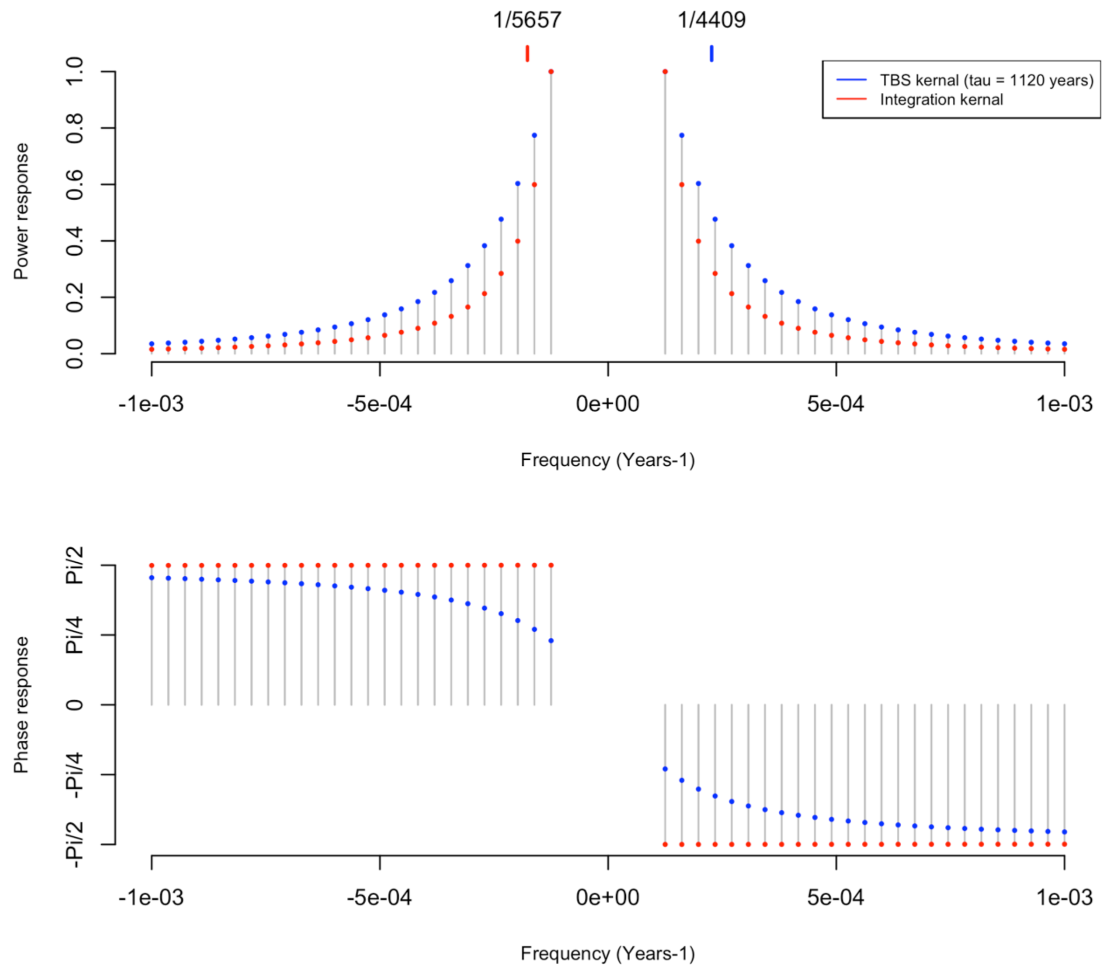

Figure S2.2. Frequency response comparison between the I/D and TBS models.

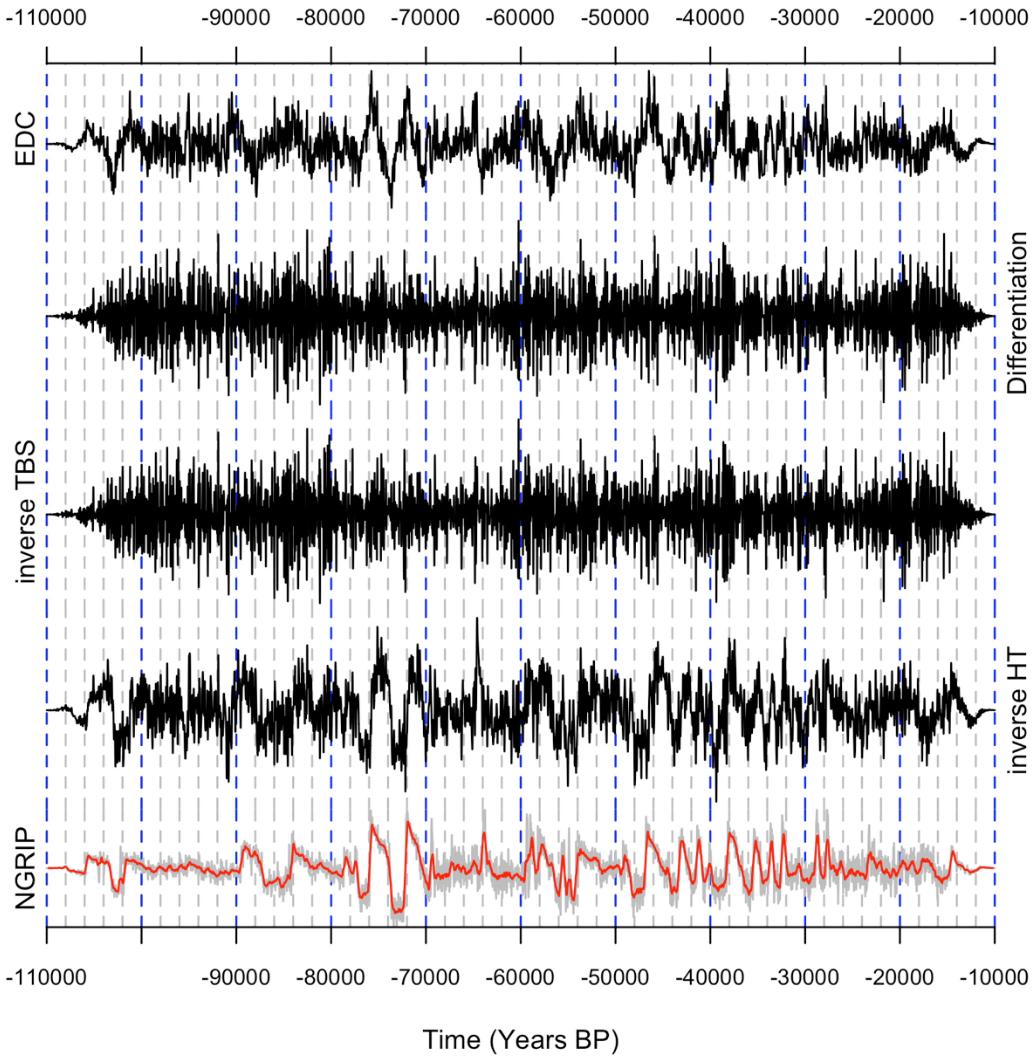

Figure S2.3. Simulation of Greenland NGRIP record from the Antarctic EDC record when the input signal did not go through the low-pass filtering.